Unusual Iron–Iron and Ruthenium–Ruthenium Single Bonds Doubly Bridged by Two $Cu(PR_3)$ Fragments: Syntheses of Iron–Copper, Iron–Silver, and Ruthenium–Copper Heterometallic Complexes and Structures of $M_2(CO)_8(\mu\text{-}CuPCy_3)_2$ (M = Fe, Ru), $[PPh_4][Fe_2(CO)_8(\mu\text{-}CuPCy_3)]$, and $[PPh_4]_2\{[Fe_2(CO)_8]_2[\mu_4\text{-}\eta^2\text{-}Cu_2(Cy_2PCH_2CH_2PCy_2)]\}$

Haibin Deng and Sheldon G. Shore*

Department of Chemistry, The Ohio State University, Columbus, Ohio 43210

Received March 6, 1991

Heterometallic tetranuclear clusters $M_2(CO)_8(\mu\text{-}M'PCy_3)_2$ (M = Fe, M' = Cu (1); M = Fe, M' = Ag (2); M = Ru, M' = Cu (3)), trinuclear clusters $X[M_2(CO)_8(\mu\text{-}M'PCy_3)]$ (X = Na, M = Fe, M' = Cu (4a); X = PPh_4, M = Fe, M' = Cu (4b); X = PPh_4, M = Fe, M' = Ag (5); X = PPh_4, M = Ru, M' = Cu (6)), and the hexanuclear complex $[PPh_4]_2\{[Fe_2(CO)_8]_2[\mu_4\text{-}\eta^2\text{-}Cu_2(Cy_2PCH_2CH_2PCy_2)]\}$ (7) are synthesized from reactions of the transition-metal carbonylates $[M_2(CO)_8]^{2-}$ (M = Fe, Ru) with mixtures of $[Cu(CH_3CN)_4][PF_6]$ or $AgBF_4$ and the phosphine ligand tricyclohexylphosphine (PCy_3) or 1,2-bis(dicyclohexylphosphino)ethane ($Cy_2PCH_2CH_2PCy_2$). The molecular structures of 1, 3, 4b·0.5THF, and 7 were determined from single-crystal X-ray data. The structures of 1 and 3 are without precedent in that they contain Fe–Fe and Ru–Ru single bonds doubly bridged by two $Cu(PCy_3)$ fragments. The four-metal cores are of the butterfly type with dihedral angles of about 150°. Furthermore, two $Cu(PCy_3)$ fragments bridge the M–M bond in an asymmetric fashion, which might be caused by a second-order Jahn–Teller effect. In 4b, the Fe–Fe bond in the $Fe_2(CO)_8$ unit is bridged by one $Cu(PCy_3)$ fragment. In 7, two $Fe_2(CO)_8$ units are connected by a $CuP(Cy_2)\text{-}CH_2CH_2(Cy_2)PCu$ moiety. Crystal data: $Fe_2(CO)_8(\mu\text{-}CuPCy_3)_2$ (1), monoclinic, space group $P2_1/c$, a = 11.042 (2) Å, b = 17.321 (3) Å, c = 24.824 (6) Å, β = 92.32 (2)°, Z = 4, and R = 0.030; $Ru_2(CO)_8(\mu\text{-}CuPCy_3)_2$ (3), monoclinic, space group $P2_1/c$, a = 11.013 (2) Å, b = 17.370 (3) Å, c = 25.169 (4) Å, β = 92.53 (1)°, Z = 4, and R = 0.022; $[PPh_4][Fe_2(CO)_8(\mu\text{-}CuPCy_3)]\cdot 0.5THF$ (4b·0.5THF) triclinic, space group $P\bar{1}$, a = 10.717 (2) Å, b = 11.703 (2) Å, c = 24.130 (7) Å, α = 90.62 (2)°, β = 92.32 (2)°, γ = 115.53 (1)°, Z = 2, and R = 0.075; $[PPh_4]_2\{[Fe_2(CO)_8]_2[\mu_4\text{-}\eta^2\text{-}Cu_2(Cy_2PCH_2CH_2PCy_2)]\}$ (7): triclinic, space group $P\bar{1}$, a = 10.810 (1) Å, b = 11.976 (1) Å, c = 18.254 (2) Å, α = 81.11 (1)°, β = 82.32 (1)°, γ = 71.40 (1)°, Z = 1, and R = 0.032.

Introduction

Transition-metal carbonylate anions play an important role in organometallic chemistry. The reaction of a transition-metal carbonylate anion with an appropriate transition-metal electrophile has proved to be a successful synthetic route to the formation of metal–metal bonds and metal clusters.[1] One of these anions, the dinuclear iron carbonylate $[Fe_2(CO)_8]^{2-}$, has been well characterized;[2] it shows rich and varied chemistry.[3] The analogous second-row and third-row transition-metal homonuclear carbonylates $[Ru_2(CO)_8]^{2-}$ and $[Os_2(CO)_8]^{2-}$ as well as the heteronuclear carbonylate $[FeRu(CO)_8]^{2-}$ were synthesized in this laboratory and described in detail recently.[4] We are presently examining the reactions of $[M_2(CO)_8]^{2-}$ (M = Fe, Ru) with appropriate electrophiles. In our initial efforts we have chosen the electrophiles $[M'(PR_3)]^+$ (M' = Cu, Ag; R = alkyl), proton analogues, since protonation of $[Fe_2(CO)_8]^{2-}$ yields the structurally characterized anion $[HFe_2(CO)_8]^-$[5] and the transient species $H_2Fe_2(CO)_8$, observed by ^1H NMR spectroscopy at low temperature.[6]

Although over 300 heterometallic clusters containing $M'(PR_3)$ (M' = Cu, Ag, Au; R = alkyl, aryl) moieties have been described,[7] none with tetranuclear cores $M_2M'_2$ (M

(1) Adams, R. D. In *The Chemistry of Metal Cluster Complexes*; Shriver, D. F., Kaesz, H. D., Adams, R. D., Eds.; VCH: New York, 1990; p 129.

(2) (a) Case, J. R.; Whiting, M. C. *J. Chem. Soc.* **1960**, 4632. (b) Griffith, W. P.; Wickham, A. *J. Chem. Soc. A* **1969**, 834. (c) Farmery, K.; Kilner, M.; Greatrex, R.; Greenwood, N. N. *J. Chem. Soc. A* **1969**, 2339. (d) Chin, H. B.; Smith, M. B.; Wilson, R. D.; Bau, R. *J. Am. Chem. Soc.* **1974**, *96*, 5285. (e) Pickett, C. J.; Pletcher, D. *J. Chem. Soc., Dalton Trans.* **1975**, 879.

(3) (a) Ruff, J. K. *Inorg. Chem.* **1968**, *7*, 1818. (b) Mason, R.; Zubieta, J. A. *J. Organomet. Chem.* **1974**, *66*, 289. (c) Dean, W. K. *J. Organomet. Chem.* **1977**, *135*, 195. (d) Collman, J. P.; Rothrock, R. K.; Finke, R. G.; Rose-Munch, F. *J. Am. Chem. Soc.* **1977**, *99*, 7381. (e) Collman, J. P.; Finke, R. G.; Matlock, P. L.; Wahren, R.; Komoto, R. G.; Brauman, J. I. *J. Am. Chem. Soc.* **1978**, *100*, 1119. (f) Sumner, C. E., Jr.; Riley, P. E.; Davis, D. E.; Petitt, R. *J. Am. Chem. Soc.* **1980**, *102*, 1752. (g) Sumner, C. E., Jr.; Collier, J. A.; Petitt, R. *Organometallics* **1982**, *1*, 1350. (h) Anema, S. G.; Barris, G. C.; Mackay, K. M.; Nicholson, B. K. *J. Organomet. Chem.* **1988**, *350*, 207.

(4) (a) Hsu, L.-Y.; Bhattacharyya, N. K.; Shore, S. G. *Organometallics* **1985**, *4*, 1483. (b) Bhattacharyya, N. K.; Coffy, T. J.; Quintana, W.; Salupo, T. A.; Bricker, J. C.; Shay, T. B.; Payne, M.; Shore, S. G. *Organometallics* **1990**, *9*, 2368.

(5) (a) Farmery, K.; Kilner, M.; Greatrex, R.; Greenwood, N. N. *Chem. Commun.* **1968**, 593. (b) Chin, H. B.; Bau, R. *Inorg. Chem.* **1978**, *17*, 2314.

(6) Krustic, P. J.; Jones, D. J.; Roe, D. C. *Organometallics* **1986**, *5*, 456.

(7) Salter, I. D. *Adv. Organomet. Chem.* **1989**, *29*, 249 and references therein.

(8) (a) Pearson, R. G. *J. Am. Chem. Soc.* **1969**, *91*, 1252. (b) Pearson, R. G. *Proc. Natl. Acad. Sci. U.S.A.* **1975**, *72*, 2104. (c) Pearson, R. G. *J. Mol. Struct.* **1983**, *103*, 25.

(9) Kubas, G. J. *Inorg. Synth.* **1979**, *19*, 90.

(10) SDP (developed by B. A. Frenz and Associates, Inc., College Station, TX 77840) was used to process X-ray data, to apply corrections, and to solve and refine the structures.

(11) (a) Rossell, O.; Seco, M.; Jones, P. G. *Inorg. Chem.* **1990**, *29*, 348. (b) Ferrer, M.; Reina, R.; Rossell, O.; Seco, M.; Solans, X. *J. Chem. Soc., Dalton Trans.* **1991**, 347.

(12) Evans, D. G.; Mingos, D. M. *J. Organomet. Chem.* **1982**, *232*, 171.

0276-7333/91/2310-3486$02.50/0

= Fe, Ru, Os; M′ = Cu, Ag, Au) have been reported.[29] Early attempts by Doyle et al. to synthesize four-metal Fe_2Cu_2 complexes were unsuccessful.[27] Recently Rossell et al. investigated the reaction of $[NEt_4]_2[Fe_2(CO)_8]$ with $ClAuPPh_3$ in a 1:2 molar ratio, but only $[NEt_4][Fe_2(CO)_8(\mu\text{-}AuPPh_3)]$ could be obtained.[11a,29] We found that syntheses of compounds with formula $M_2(CO)_8(M'PR_3)_2$ can be achieved only with certain phosphine ligands, such as PCy_3 or P(*tert*-butyl)$_3$.[28] With the ligands P(*n*-butyl)$_3$, PPh_3, and P(*o*-tolyl)$_3$ copper metal and intractable materials result. Steric or electronic requirements for clusters with M_2M' cores appear to be less demanding. For example, $[Fe_2(CO)_8(CuPR_3)]^-$ can be obtained with P(*n*-butyl)$_3$[28] as well as PCy_3; Rossell and co-workers have also prepared $[NEt_4][Fe_2(CO)_8(\mu\text{-}CuPPh_3)]$.[11b]

In this paper we report the syntheses of the new mixed-metal tetranuclear clusters $M_2(CO)_8(\mu\text{-}M'PCy_3)_2$ (M = Fe, M′ = Cu (**1**); M = Fe, M′ = Ag (**2**); M = Ru, M′ = Cu (**3**)), trinuclear clusters $X[M_2(CO)_8(\mu\text{-}M'PCy_3)]$ (X = Na, M = Fe, M′ = Cu (**4a**); X = PPh_4, M = Fe, M′ = Cu (**4b**); X = PPh_4, M = Fe, M′ = Ag (**5**); X = PPh_4, M = Ru, M′ = Cu (**6**); Cy = cyclohexyl), and the hexanuclear complex $[PPh_4]_2[[Fe_2(CO)_8]_2[\mu_4\text{-}\eta^2\text{-}Cu_2(Cy_2PCH_2CH_2PCy_2)]]$ (**7**) and the molecular structures of **1**, **3**, **4b**, and **7**. In addition, the reactions of iron–copper tetranuclear and trinuclear clusters **1** and **4** with simple electrophiles and nucleophiles are discussed.

The molecular structures of **1** and **3** are without precedent in that they contain Fe–Fe and Ru–Ru *single* bonds doubly bridged by two $Cu(PCy_3)$ fragments. Furthermore, two $Cu(PCy_3)$ fragments bridge the M–M bond in an asymmetric fashion, which may be caused by a second-order Jahn–Teller effect.[8] A qualitative analysis of this distortion is therefore put forth in this paper.

Experimental Section

General Comments. All manipulations were carried out on a standard high-vacuum line or in a drybox under an atmosphere of dry, pure N_2. Tetrahydrofuran (THF) and Et_2O were dried by distillation from sodium–benzophenone ketyl into storage bulbs equipped with Teflon stopcocks and containing sodium–benzophenone ketyl. CH_3CN and CH_2Cl_2 were dried over P_4O_{10} with continuous stirring for 2–3 days followed by distillation into storage bulbs. Hexane was stirred over concentrated H_2SO_4 for 2–3 days followed by extraction with distilled water and then dried over CaH_2 and sodium. Pyridine was dried over sodium and distilled prior to use.

$AgBF_4$, PCy_3, $Cy_2PCH_2CH_2PCy_2$, and $HBF_4\cdot OEt_2$ (Strem Chemicals) were used as received. KH in oil (Strem Chemicals) was washed with hexane to remove oil and dried under vacuum. Its activity was determined to be 91% by measuring the amount of H_2 released when it reacted with ethanol. $[Cu(CH_3CN)_4][PF_6]$,[9] $Na_2[Fe_2(CO)_8]$,[4b] $[PPh_4]_2[Fe_2(CO)_8]$,[4b] and $[PPh_4]_2[Ru_2(CO)_8]$[4b] were prepared by procedures reported in the literature.

All IR spectra were recorded with 2-cm^{-1} resolution on a Mattson-Polaris FT-IR spectrometer. Solution spectra were obtained in Perkin-Elmer liquid cells with 0.1-mm Teflon spacers and KBr windows. Proton NMR (δ(TMS) = 0.00 ppm), ^{31}P NMR (δ(85% H_3PO_4) = 0.00 ppm), and ^{13}C NMR (δ(TMS) = 0.00 ppm) spectra were obtained on either a Bruker AM-250 NMR spectrometer operating at 250.14, 101.25, and 62.90 MHz or a Bruker AC-300 NMR spectrometer operating at 300.13, 121.50, and 75.47 MHz, respectively. Elemental analyses were performed by Oneida Research Services, Whitesboro, NY.

Preparation of $Fe_2(CO)_8(\mu\text{-}CuPCy_3)_2$ (1). Method A. In the drybox, 293 mg (1.046 mmol) of PCy_3 and 390 mg (1.047 mmol) of $[Cu(CH_3CN)_4]PF_6$ were dissolved in 15 mL of dry CH_3CN; 5 mL of CH_3CN solution containing 200 mg (0.524 mmol) of $Na_2[Fe_2(CO)_8]$ was added dropwise to the former while it was stirred. The solution turned green immediately, and a dark green precipitate formed. After all the $Na_2[Fe_2(CO)_8]$ was added, the solution was stirred for another 10 min and then filtered. The precipitate collected on the frit was washed five times with CH_3CN and dried under vacuum; yield 410 mg, 76%.

Method B. In the drybox, 166 mg (0.593 mmol) of PCy_3 and 221 mg (0.593 mmol) of $[Cu(CH_3CN)_4]PF_6$ were dissolved in 15 mL of dry CH_3CN in a flask; 5 mL of CH_3CN solution containing 315 mg (0.311 mmol) of $[PPh_4]_2[Fe_2(CO)_8]$ was added dropwise to the former while it was stirred. The solution turned green immediately, and a mixture of dark green and white precipitates formed. After all the $[PPh_4]_2[Fe_2(CO)_8]$ was added, the flask was connected to a vacuum line extractor and brought out of the drybox. The solution was stirred for another 15 min, and CH_3CN was then removed under vacuum. A 15-mL portion of dry toluene was condensed into the flask at −78 °C. The product was dissolved in toluene, and the solution was filtered, leaving white $[PPh_4][PF_6]$ on the glass frit. The solvent was pumped away, and the collection flask was connected to a fresh extractor in the drybox. A minimal amount of CH_3CN was condensed into the flask at −78 °C, and the solid was washed again with CH_3CN and filtered. The product was collected on the frit and dried under vacuum; yield 233 mg, 77%. Anal. Calcd for $C_{44}H_{66}Cu_2Fe_2O_8P_2$: C, 51.62; H, 6.45. Found: C, 51.58; H, 6.49. IR (THF, ν_{CO}, cm^{-1}): 2027 (w), 1986 (s), 1944 (m, sh), 1921 (s). ^{1}H NMR (THF-d_8, 303 K, δ (ppm)): 1.30–2.04 (complex m, C_6H_{11}). ^{31}P{^{1}H} NMR (THF-d_8, 303 K, δ (ppm)): 16.55 (s). ^{13}C{^{1}H} NMR (THF-d_8, 303 K, δ (ppm)): 214.29 (t, $^3J_{PC}$ = 2.3 Hz, CO); 32.87 (d, $^1J_{PC}$ = 17.5 Hz), 31.10 (d, $^3J_{PC}$ = 1.6 Hz), 28.23 (d, $^2J_{PC}$ = 11.2 Hz), 26.95 (s) (C_6H_{11}).

Preparation of $Fe_2(CO)_8(\mu\text{-}AgPCy_3)_2$ (2). The preparation is similar to method B for the preparation of $Fe_2(CO)_8(\mu\text{-}CuPCy_3)_2$ (**1**). Thus, a reaction involving 92 mg (0.473 mmol) of $AgBF_4$, 133 mg (0.475 mmol) of PCy_3, and 240 mg (0.237 mmol) of $[PPh_4]_2[Fe_2(CO)_8]$ yields 160 mg of **2** (61%). Anal. Calcd for $C_{44}H_{66}Ag_2Fe_2O_8P_2$: C, 46.84; H, 5.90. Found: C, 47.16; H, 6.36. IR (THF, ν_{CO}, cm^{-1}): 2025 (w), 1980 (s), 1924 (s). ^{1}H NMR (THF-d_8, 303 K, δ (ppm)): 1.29–2.01 (complex m, C_6H_{11}). ^{31}P{^{1}H} NMR (THF-d_8, 303 K, δ (ppm)): 37.38 (2 d, $^1J_{^{109}AgP}$ = 531 Hz, $^1J_{^{107}AgP}$ = 460 Hz). ^{13}C{^{1}H} NMR (THF-d_8, 303 K, δ (ppm)): 216.34

(13) Braunstein, P.; Rose, J.; Dedieu, A.; Dusausoy, Y.; Mangeot, J.-P.; Tiripicchio, A.; Tiripicchio-Camellini, M. *J. Chem. Soc., Dalton Trans.* **1986**, 225.
(14) Bennett, M. J.; Graham, W. A. G.; Hoyano, J. K.; Hutcheon, W. L. *J. Am. Chem. Soc.* **1972**, *94*, 6232.
(15) (a) Churchill, M. R.; Chang, S. W.-Y. *Inorg. Chem.* **1974**, *13*, 2413. (b) Wei, C.-Y.; Marks, M. W.; Bau, R.; Kirtley, S. W.; Bisson, D. E.; Henderson, M. E.; Koetzle, T. F. *Inorg. Chem.* **1982**, *21*, 2556.
(16) (a) Orpen, A. G.; Rivera, A. V.; Bryan, E. G.; Pippard, D.; Sheldrick, G. M.; Rouse, K. D. *J. Chem. Soc., Chem. Commun.* **1978**, 723. (b) Broach, R. W.; Williams, J. M. *Inorg. Chem.* **1979**, *18*, 314. (c) Sherwood, D. E.; Hall, M. B. *Inorg. Chem.* **1982**, *21*, 3458.
(17) Burgess, K.; Johnson, B. F. G.; Kaner, D. A.; Lewis, J.; Raithby, P. R.; Azman, S. N.; Syed-Mustaffa, B. *J. Chem. Soc., Chem. Commun.* **1983**, 455.
(18) Riera, V.; Ruiz, M. A.; Tiripicchio, A.; Camellini, M. T. *J. Chem. Soc., Chem. Commun.* **1985**, 1505.
(19) Two M′(PR$_3$) fragments may doubly bridge a metal–metal edge of a polynuclear clsuter, where direct M′–M′ interactions are always present and M′ is Au in most cases.[7]
(20) Cotton, F. A.; Fang, A. *J. Am. Chem. Soc.* **1982**, *104*, 113.
(21) (a) Chisholm, M. H.; Cotton, F. A.; Fang, A.; Kober, E. M. *Inorg. Chem.* **1984**, *23*, 749. (b) Jiang, Y.; Tang, A.; Hoffmann, R.; Huang, J.; Lu, J. *Organometallics* **1985**, *4*, 27. (c) Chisholm, M. H.; Clark, D. L.; Folting, K.; Huffman, J. C.; Hampden-Smith, M. *J. Am. Chem. Soc.* **1987**, *109*, 7750.
(22) (a) Hoffmann, R. *Science (Washington, D.C.)* **1981**, *211*, 995. (b) Hoffmann, R. *Angew. Chem., Int. Ed. Engl.* **1982**, *21*, 711.
(23) Longuet-Higgins, H. C. *Q. Rev., Chem. Soc.* **1957**, *11*, 121.
(24) Mingos, D. M. P.; May, A. S. In *The Chemistry of Metal Cluster Complexes*; Shriver, D. F., Kaesz, H. D., Adams, R. D., Eds.; VCH: New York, 1990; p 31.
(25) Doyle, G.; Eriksen, K. A.; Engen, D. V. In *Biological & Inorganic Copper Chemistry*; Karlin, K. D., Zubieta, J., Eds.; Adenine Press: Guilderland, NY, 1985.
(26) Crabtree, R. H., Lavin, M. *Inorg. Chem.* **1986**, *25*, 805.
(27) Doyle, G.; Eriksen, K. A.; Engen, D. V. *J. Am. Chem. Soc.* **1985**, *107*, 7914.
(28) Deng, H. Ph.D. Dissertation, The Ohio State University, 1991.
(29) Note added in proof. Very recently the preparation and crystal structure of $Fe_2Au_2(CO)_8(\mu\text{-dppm})$ with the approximate four-metal square geometry were reported. See: Alvarez, S.; Rossell, O.; Seco, M.; Valls, J.; Pellinghelli, M. A.; Tiripicchio, A. *Organometallics* **1991**, *10*, 2309.

(s, CO); 32.74 ($^1J_{PC}$ = 13.6 Hz), 31.78 (d, $^3J_{PC}$ = 3.8 Hz), 28.08 (d, $^2J_{PC}$ = 11.6 Hz), 26.83 (s) (C_6H_{11}).

Preparation of $Ru_2(CO)_8(\mu\text{-}CuPCy_3)_2$ (3). The preparation is similar to method B for the preparation of $Fe_2(CO)_8(\mu\text{-}CuPCy_3)_2$ (1). Thus, a reaction involving 148 mg (0.134 mmol) of $[PPh_4]_2[Ru_2(CO)_8]$, 75 mg (0.268 mmol) of PCy_3, and 100 mg (0.268 mmol) of $[Cu(CH_3CN)_4]PF_6$ yields 100 mg of **3** (67%). Anal. Calcd for $C_{44}H_{66}Cu_2O_8P_2Ru_2$: C, 47.43; H, 5.97. Found: C, 47.61; H, 6.08. IR (THF, ν_{CO}, cm^{-1}): 2055 (w), 2000 (s), 1967 (s), 1937 (s). ^{1}H NMR (THF-d_8, 303 K, δ (ppm)): 1.24–2.01 (complex m, C_6H_{11}). ^{31}P{^{1}H} NMR (THF-d_8, 303 K, δ (ppm)): 16.61 (s). ^{13}C{^{1}H} NMR (THF-d_8, 303 K, δ (ppm)): 207.08 (t, $^3J_{PC}$ = 2.3 Hz, CO); 33.35 (d, $^1J_{PC}$ = 16.4 Hz), 31.30 (d, $^3J_{PC}$ = 2.5 Hz), 28.29 (d, $^2J_{PC}$ = 11.1 Hz), 26.99 (s) (C_6H_{11}).

Preparation of $Na[Fe_2(CO)_8(\mu\text{-}CuPCy_3)]$ (4a). In the drybox, 360 mg (0.942 mmol) of $Na_2[Fe_2(CO)_8]$ was placed in a flask containing a stirbar and was dissolved in 5 mL of dry CH_3CN; 293 mg (0.786 mmol) of $[Cu(CH_3CN)_4][PF_6]$ and 220 mg (0.786 mmol) of PCy_3 were dissolved in 5 mL of CH_3CN in a glass vial. The latter solution was added dropwise to the former while it was stirred. A red solution was obtained. The flask was connected to an extractor and brought out of the drybox. It was evacuated, and CH_3CN was removed under vacuum. A 15-mL portion of dry Et_2O was condensed into the flask at −78 °C, and the solution was filtered, leaving a pink precipitate (mixture of $Na[PF_6]$ and excess $Na_2[Fe_2(CO)_8]$) on the frit. Et_2O was then removed under vacuum. The solid was scraped from the flask in the drybox. Elemental analysis as well as NMR data shows the presence of solvent molecules CH_3CN, which cannot be removed under vacuum at room temperature; yield 560 mg, 98% based on $[Cu(CH_3CN)_4]PF_6$. Anal. Calcd for $C_{27}H_{34.5}CuFe_2N_{0.5}NaO_8P$ ($Na[Fe_2(CO)_8(\mu\text{-}CuPCy_3)]\cdot 0.5CH_3CN$): C, 44.84; H, 4.81; N, 1.08. Found: C, 44.51; H, 4.82; N, 1.08. IR (THF, ν_{CO}, cm^{-1}): 2006 (m), 1985 (m), 1970 (m), 1951 (s), 1911 (s), 1901 (s), 1770 (w), 1752 (w), 1713 (w). ^{1}H NMR (THF-d_8, 303 K, δ (ppm)): 1.29–2.03 (complex m, C_6H_{11} and CH_3CN). ^{31}P{^{1}H} NMR (THF-d_8, 303 K, δ (ppm)): 14.38 (s). ^{13}C{^{1}H} NMR (THF-d_8, 303 K, δ (ppm)): 224.45 (d, $^3J_{PC}$ = 1.8 Hz, CO); 33.07 (d, $^1J_{PC}$ = 15.3 Hz), 30.98 (d, $^3J_{PC}$ = 3.2 Hz), 28.42 (d, $^2J_{PC}$ = 11.2 Hz), 27.07 (s) (C_6H_{11}); 0.67 (s, CH_3CN, the other resonance at δ ~118 (br) ppm was not resolved).

Preparation of $[PPh_4][Fe_2(CO)_8(\mu\text{-}CuPCy_3)]$ (4b). In the drybox, 315 mg (0.311 mmol) of $[PPh_4]_2[Fe_2(CO)_8]$ was placed in a flask containing a stirbar and was dissolved in 5 mL of dry CH_3CN; 110 mg (0.295 mmol) of $[Cu(CH_3CN)_4][PF_6]$ and 83 mg (0.296 mmol) of PCy_3 were dissoved in 5 mL of CH_3CN in a glass vial. The latter solution was added dropwise to the former while it was stirred. A red solution was obtained with some white precipitate. The flask was connected to an extractor and brought out of the drybox. It was evacuated, and CH_3CN was removed under vacuum. A 5-mL portion of dry THF was condensed into the flask at −78 °C, and the solution was filtered, leaving white $[PPh_4][PF_6]$ on the frit. A clean extractor was connected to the collection flask in the drybox. THF solvent was then removed under vacuum, leaving a brown solid in the flask. (Note: In some instances, THF solvent could not be totally removed from the solid and an oily material was obtained. CH_2Cl_2 may be used to redissolve the oily material. A dry solid then results when the solvents are pumped away). A 15-mL amount of dry hexane was condensed into the flask at −78 °C. The suspension was filtered, and the product was collected on the frit and dried under vacuum; yield 250 mg, 83% based on $[Cu(CH_3CN)_4]PF_6$. Anal. Calcd for $C_{50}H_{53}CuFe_2O_8P_2$: C, 58.93; H, 5.24. Found: C, 59.13; H, 5.28. IR (CH_3CN, ν_{CO}, cm^{-1}): 2008 (m), 1975 (w, sh), 1952 (s), 1898 (s), 1850 (m, sh), 1742 (w). IR (crystals in Nujol mull, ν_{CO}, cm^{-1}): 2007 (m), 1948 (s), 1895 (s, br), 1871 (s, sh), 1842 (m, sh), 1736 (w). ^{1}H NMR (THF-d_8, 303 K, δ (ppm)): 7.72–7.96 (complex m, C_6H_5), 1.28–2.03 (complex m, C_6H_{11}). ^{31}P{^{1}H} NMR (THF-d_8, 303 K, δ (ppm)): 22.17 (s, $[PPh_4]^+$), 13.72 (s). ^{13}C{^{1}H} NMR (THF-d_8, 303 K, δ (ppm)): 221.73 (d, $^3J_{PC}$ = 1.9 Hz, CO); 136.37 (d, $^4J_{PC}$ = 3.5 Hz), 135.62 (d, $^3J_{PC}$ = 10.6 Hz), 131.37 (d, $^2J_{PC}$ = 12.9 Hz), 119.10 (d, $^1J_{PC}$ = 89.3 Hz) (C_6H_5); 33.12 (d, $^1J_{PC}$ = 14.5 Hz), 30.96 (d, $^3J_{PC}$ = 3.4 Hz), 28.50 (d, $^2J_{PC}$ = 11.3 Hz), 27.20 (s) (C_6H_{11}). ^{13}C{^{1}H} NMR (THF-d_8, 213 K, δ (ppm)): 223.66 (s, CO).

Preparation of $[PPh_4][Fe_2(CO)_8(\mu\text{-}AgPCy_3)]$ (5). The preparation of **5** follows the same procedure as that of **4b**. Thus, a reaction involving 58 mg (0.298 mmol) of $AgBF_4$, 85 mg (0.304 mmol) of PCy_3, and 360 mg (0.355 mmol) of $[PPh_4]_2[Fe_2(CO)_8]$ yields 280 mg of **5**, 88% based on $AgBF_4$. Anal. Calcd for $C_{50}H_{53}AgFe_2O_8P_2$: C, 56.47; H, 5.02. Found: C, 57.41; H, 4.78. IR (CH_3CN, ν_{CO}, cm^{-1}): 2001 (m), 1951 (s), 1904 (vs), 1733 (m). ^{1}H NMR (THF-d_8, 303 K, δ (ppm)): 7.73–7.96 (complex m, C_6H_5); 1.26–1.99 (complex m, C_6H_{11}). ^{31}P{^{1}H} NMR (THF-d_8, 303 K, δ (ppm)): 34.04 (2 d, $^1J_{^{109}Ag-P}$ = 460 Hz, $^1J_{^{107}Ag-P}$ = 398 Hz), 22.13 (s, $[PPh_4]^+$). ^{13}C{^{1}H} (THF-d_8, 303 K, δ (ppm)): 231.48 (d, $^2J_{^{109,107}Ag-C}$ = 4.5 Hz, CO); 136.37 (s), 135.66 (d, $^3J_{PC}$ = 10.4 Hz), 131.37 (d, $^2J_{PC}$ = 12.9 Hz), 119.13 (d, $^1J_{PC}$ = 89.4 Hz) (C_6H_5); 32.83 (m), 31.56 (d, $^3J_{PC}$ = 5.3 Hz), 28.21 (d, $^2J_{PC}$ = 11.3 Hz), 26.88 (s) (C_6H_{11}).

Preparation of $[PPh_4][Ru_2(CO)_8(\mu\text{-}CuPCy_3)]$ (6). The synthesis is similar to that of **4b**. Thus, a reaction involving 700 mg (0.633 mmol) of $[PPh_4]_2[Ru_2(CO)_8]$, 150 mg (0.536 mmol) of PCy_3, and 200 mg (0.537 mmol) of $[Cu(CH_3CN)_4][PF_6]$ results in 363 mg of **6**, 61% based on $[Cu(CH_3CN)_4]PF_6$. Anal. Calcd for $C_{50}H_{53}CuO_8P_2Ru_2$: C, 54.12; H, 4.81. Found: C, 54.13; H, 4.83. IR (CH_3CN, ν_{CO}, cm^{-1}): 2052 (w), 2019 (w), 1966 (s), 1925 (s), 1860 (m, sh), 1730 (w, br). ^{1}H NMR (THF-d_8, 303 K, δ (ppm)): 7.64–7.95 (complex m, C_6H_5); 1.22–1.87 (complex m, C_6H_{11}). ^{31}P{^{1}H} NMR (THF-d_8, 303 K, δ (ppm)): 22.13 (s, $[PPh_4]^+$), 14.61 (s). ^{13}C{^{1}H} NMR (THF-d_8, 303 K, δ (ppm)): 212.20 (d, $^3J_{PC}$ = 2.3 Hz, CO); 136.39 (d, $^4J_{PC}$ = 3.3 Hz), 135.63 (d, $^3J_{PC}$ = 10.1 Hz), 131.39 (d, $^2J_{PC}$ = 12.9 Hz), 119.10 (d, $^1J_{PC}$ = 89.3 Hz) (C_6H_5); 33.24 (d, $^1J_{PC}$ = 14.0 Hz), 31.07 (d, $^3J_{PC}$ = 3.6 Hz), 28.50 (d, $^2J_{PC}$ = 10.6 Hz), 27.20 (s) (C_6H_{11}).

Preparation of $[PPh_4]_2\{[Fe_2(CO)_8]_2[\mu_4\text{-}\eta^2\text{-}Cu_2(Cy_2PCH_2CH_2PCy_2)]\}$ (7). The synthesis is similar to that of **4b**. Thus, a reaction involving 315 mg (0.311 mmol) of $[PPh_4]_2[Fe_2(CO)_8]$, 110 mg (0.295 mmol) of $[Cu(CH_3CN)_4]PF_6$, and 62.5 mg (0.148 mmol) of $Cy_2PCH_2CH_2PCy_2$ yields 217 mg of **7** (77% based on $[Cu(CH_3CN)_4]PF_6$). Anal. Calcd for $C_{90}H_{88}Cu_2Fe_4O_{16}P_4$: C, 56.89; H, 4.67. Found: C, 56.52; H, 4.32. IR (CH_3CN, ν_{CO}, cm^{-1}): 2008 (w), 1970 (m, sh), 1953 (s), 1899 (s), 1860 (w, sh), 1741 (vw). IR (crystals in Nujol mull, ν_{CO}, cm^{-1}): 2004 (m), 1944 (s), 1916 (m, sh), 1890 (s), 1877 (s), 1867 (s), 1840 (m), 1819 (m), 1734 (w). ^{1}H NMR (THF-d_8, 303 K, δ (ppm)): 7.63–7.93 (complex m, C_6H_5); 1.14–2.14 (complex m, C_6H_{11} and CH_2). ^{31}P{^{1}H} NMR (THF-d_8, 303 K, δ (ppm)): 22.32 (s, $[PPh_4]^+$), 10.29 (s). ^{13}C{^{1}H} NMR (THF-d_8, 303 K, δ (ppm)): 221.98 (s, CO); 136.40 (d, $^4J_{PC}$ = 3.5 Hz), 135.71 (d, $^3J_{PC}$ = 10.6 Hz), 131.34 (d, $^2J_{PC}$ = 12.9 Hz), 119.10 (d, $^1J_{PC}$ = 89.3 Hz) (C_6H_5); 34.00 (m), 30.04 (s), 29.07 (s), 27.80 (m), 26.83 (s) (C_6H_{11} and CH_2). ^{13}C{^{1}H} NMR (THF-d_8, 193 K, δ (ppm)): 222.23 (s, CO).

X-ray Crystal Structure Determination. Single crystals of **1** (green) and **3** (orange) were grown by cooling saturated hexane solutions of these compounds. Single crystals of **4b**·0.5THF and **7** (both red) were grown by slow diffusion of Et_2O into the saturated THF solutions. Crystals of suitable size were mounted under N_2 in glass capillaries. All crystallographic data were collected on an Enraf-Nonius CAD4 diffractometer with graphite-monochromated Mo Kα radiation. Unit cell parameters were obtained by a least-squares refinement of the angular settings from 25 reflections, well distributed in reciprocal space and lying in a 2θ range of 24–30°. Crystallographic data are given in Table I. The diffraction symmetry (C_{2h}, $2/m$) and the systematic absences ($h0l$ for $l = 2n + 1$; $0k0$ for $k = 2n + 1$) for **1** and **3** uniquely determine the space group $P2_1/c$ (No. 14). The structures of **1** and **3** are isomorphous. The space group for **4b**·0.5THF and **7** is $P\bar{1}$ (No. 2), as the unit cells are triclinic and the diffraction statistics favor centrosymmetric space groups.

All data were corrected for Lorentz and polarization effects, decay, and absorption (empirically from ψ-scan data). All structures were solved by employing a combination of MULTAN 11/82 and difference Fourier techniques with analytical scattering factors used throughout the structure refinement and both real and imaginary components of the anomalous dispersion included for all non-hydrogen atoms. All the crystallographic computations were carried out on PDP 11/44 and DEC Vax station 3100 computers, using the Structure Determination Package (SDP).[10] After all of the non-hydrogen atoms were located and refined, the hydrogen atoms of the phosphine groups were placed at calculated positions (C–H = 0.95 Å, B(H) = 1.3B(C) Å^2). Then with the positional and thermal parameters of all of the hydrogens fixed, the non-hydrogen atoms were refined anisotropically. New hy-

Table I. Crystal Data for $Fe_2(CO)_8(\mu\text{-}CuPCy_3)_2$ (1), $Ru_2(CO)_8(\mu\text{-}CuPCy_3)_2$ (3), $[PPh_4][Fe_2(CO)_8(\mu\text{-}CuPCy_3)]\cdot 0.5THF$ (4b·0.5THF), and $[PPh_4]_2[Fe_2(CO)_8]_2[\mu_4\text{-}\eta^2\text{-}Cu_2(Cy_2PCH_2CH_2PCy_2)]$ (7)

	1	3	4b·0.5THF	7
formula	$C_{44}H_{66}Cu_2Fe_2O_8P_2$	$C_{44}H_{66}Cu_2O_8P_2Ru_2$	$C_{52}H_{57}CuFe_2O_{8.5}P_2$	$C_{90}H_{88}Cu_2Fe_4O_{16}P_4$
mol wt	1023.75	1114.19	1055.22	1900.06
space group	$P2_1/c$	$P2_1/c$	$P\bar{1}$	$P\bar{1}$
a, Å	11.042 (2)	11.013 (2)	10.717 (2)	10.810 (1)
b, Å	17.321 (3)	17.370 (3)	11.703 (2)	11.976 (1)
c, Å	24.824 (6)	25.169 (4)	24.130 (7)	18.254 (2)
α, deg	90	90	90.62 (2)	81.11 (1)
β, deg	92.32 (2)	92.53 (1)	101.00 (2)	82.32 (1)
γ, deg	90	90	115.53 (1)	71.40 (1)
vol (unit cell), Å^3	4743.7	4809.9	2665.7	2203.9
molecules/unit cell	4	4	2	1
D(calc), g cm^{-3}	1.433	1.539	1.315	1.432
cryst dimens, mm	0.23 × 0.31 × 0.38	0.38 × 0.62 × 0.69	0.25 × 0.30 × 0.40	0.35 × 0.40 × 0.50
temp, °C	25	−50	25	25
radiatn (λ, Å)	Mo Kα (0.710730)	Mo Kα (0.710730)	Mo Kα (0.710730)	Mo Kα (0.710730)
abs coeff, cm^{-1}	16.001	15.916	10.391	12.493
max transmission, %	99.98	99.80	99.86	99.95
min transmission, %	89.32	85.13	76.87	77.40
2θ limits, deg	4–45	4–45	4–45	4–45
scan mode	ω–2θ	ω–2θ	ω–2θ	ω–2θ
no. of rflns measd	6565	6647	7407	6116
no. of unique rflns	5511	5998	5945	5332
no. of unique rflns >3$\sigma(I)$	3515	5068	3810	4165
no. of variables	524	524	579	523
R_F	0.030	0.022	0.075	0.032
R_{wF}	0.037	0.030	0.098	0.044
GOF	1.215	1.465	2.531	1.668

drogen positions were calculated again, and this procedure was repeated until the parameters of non-hydrogen atoms were refined to convergence (final shift/error ≤0.03). In the solution of the structure of **4b**·0.5THF, the residual electron densities in the difference Fourier maps were assigned as the THF molecule of solvation, which was disordered in two orientations. Each orientation was assigned 0.25 occupancy so that the thermal parameters of these atoms could be refined to reasonable values. The highest residual peaks on the final difference Fourier maps for **1**, **3**, **4b**·0.5THF, and **7** are 0.55, 0.41, 1.12, and 0.39 e/Å^3, respectively.

Reaction of 1 with $Na_2[Fe_2(CO)_8]$. A 30-mg (0.029-mmol) amount of **1** and 11 mg (0.029 mmol) of $Na_2[Fe_2(CO)_8]$ were placed in a NMR tube in the drybox. THF-d_8 was used as a solvent. The tube was flame-sealed. ^{31}P and ^{13}C NMR spectra showed that only **4a** was present in solution.

Reaction of 1 with Pyridine. In the drybox, 50 mg (0.049 mmol) of **1** was placed in a flask. The flask was connected to a vacuum adaptor and brought out of the drybox. After evacuation of the flask, 5 mL of pyridine was condensed into the flask at −78 °C. The green color of **1** changed to red immediately. IR (pyridine, ν_{CO}, cm^{-1}); 2006 (m), 1975 (w, sh), 1949 (s), 1894 (s), 1856 (m, sh), 1743 (w). This infrared spectrum is almost identical with that of **4b** in CH_3CN. Pyridine was pumped away under dynamic vacuum over 3 h, and the color of the solid changed back to green. The infrared spectrum of the pyridine-free solid in THF confirmed that the solid was **1**.

In a separate experiment, 40 mg (0.039 mmol) of **1** was placed in a NMR tube and pyridine-d_5 was used as the solvent. The green color of **1** changed to red immediately. ^{31}P and ^{13}C NMR spectra were obtained. $^{31}P\{^1H\}$ NMR (pyridine-d_5, 303 K, δ (ppm)): 14.93 (s), 12.30 (s) (two peaks overlapped). $^{31}P\{^1H\}$ NMR (pyridine-d_5, 243 K, δ (ppm)): 15.35 (s), 10.95 (s), with approximate 1:1 integration ratio. $^{13}C\{^1H\}$ NMR (pyridine-d_5, 303 K, δ (ppm)): 222.74 (s, CO); 32.73 (d, $^1J_{PC}$ = 14.9 Hz), 30.68 (d, $^3J_{PC}$ = 3.4 Hz), 27.74 (d, $^2J_{PC}$ = 10.8 Hz), 26.52 (s) (C_6H_{11}).

In comparison, the NMR spectra of **4b** in pyridine-d_5 are as follows. $^{31}P\{^1H\}$ NMR (pyridine-d_5, 303 K, δ (ppm)): 22.20 (s, $[PPh_4]^+$), 15.07 (s). $^{13}C\{^1H\}$ NMR (pyridine-d_5, 303 K, δ (ppm)): 222.95 (s, CO); 32.60 (d, $^1J_{PC}$ = 15.3 Hz), 30.60 (d, $^3J_{PC}$ = 3.1 Hz), 27.84 (d, $^2J_{PC}$ = 10.8 Hz), 26.53 (s) (C_6H_{11}).

Reaction of 1 with KH. In the drybox 50 mg (0.049 mmol) of **1** and 5 mg (91% active, 0.114 mmol) of KH were placed in a NMR tube that was connected to a vacuum adaptor. THF-d_8 was condensed into the tube at −78 °C. The tube was then flame-sealed. Gas evolution occurred at −78 °C. The tube was kept at −78 °C prior to NMR experiments. The reaction was monitored by ^{31}P NMR spectroscopy. At low temperature (−78 to 0 °C) some unidentified species were observed in addition to **4d** and free PCy_3. When the NMR sample was warmed to room temperature, only **4d** and PCy_3 were present. After 24 h, the resonance due to **4d** decreased to the base line while that of PCy_3 increased.

In another experiment, 100 mg (0.098 mmol) of **1** and 10 mg (91% active, 0.228 mmol) of KH in 20 mL of THF were stirred overnight at room temperature. The gas evolved during the reaction was measured to be 0.091 mmol (93%) with a Toepler pump. The reaction mixture was filtered. The infrared spectrum of the filtrate showed the presence of $[Fe_2(CO)_8]^{2-}$ ions. THF was removed from the filtrate, and THF-d_8 was used to prepare a NMR sample. ^{31}P and ^{13}C NMR spectra showed that free PCy_3 and $Fe_2(CO)_8^{2-}$ were only species present. The black precipitate from the filtration was not soluble in any common organic solvent. It reacts with concentrated HNO_3, and the solution turns blue-green. Addition of concentrated $NH_3\cdot H_2O$ turns the solution to deep blue, characteristics of $[Cu(NH_3)_4]^{2+}$.

Reaction of 1 with Na/Hg. In the drybox, 100 mg (0.098 mmol) of **1** was dissolved in 25 mL of dry Et_2O; 5 mg (0.217 mmol) of freshly cut Na was dissolved in 5 mL of Hg in a flask with a stirbar. The former solution was added to the Na amalgam. The mixture was stirred for 1 h, during which time a yellow-gray precipitate formed and the green solution turned orange. The suspension was transferred to a clean flask, which was then connected to an extractor. The suspension was filtered. Et_2O was then removed under vacuum. The orange residue was dissolved in THF-d_8, and the NMR spectrum of the solution showed that it contained only PCy_3 and **4a**. The solid collected on the frit was partially soluble in THF, which showed the IR absorptions due to $Na_2[Fe_2(CO)_8]$. The insoluble part was copper particles.

In a similar reaction, the mixture was stirred for 6 h and worked up the same way as above. PCy_3 was the only phosphorus-containing compound in the Et_2O filtrate. The precipitate contained Cu and $Na_2[Fe_2(CO)_8]$.

Reaction of 1 with $HBF_4\cdot OEt_2$. In the drybox 150 mg (0.146 mmol) of **1** was dissolved in 25 mL of dry Et_2O in a flask containing a stirbar; 50 mg (0.309 mmol) of $HBF_4\cdot Et_2O$ was weighed in a vial and diluted with 5 mL of Et_2O. The latter was added dropwise to the former while it was stirred. The solution was stirred for another 2 h, during which time copper-colored material precipitated out of the solution, and some of it coated the flask. The solution was filtered. The filtrate was green, and its IR spectrum showed that the major material present in solution was

$Fe_3(CO)_{12}$. A fresh collection flask was attached to the extractor in the drybox. After evacuation 3 mL of CH_3CN was condensed into the extractor. The precipitate was washed with CH_3CN, and the solution was filtered. The filtrate contained $[HPCy_3][BF_4]$, as evidenced by ^{31}P and ^1H NMR spectroscopy. ^1H NMR (CD_3CN, 303 K, δ (ppm)): 5.23 (d, $^1J_{PH}$ = 459 Hz, $[HPCy_3]^+$); 1.26–1.96 (complex m, C_6H_{11}). ^{31}P NMR (CD_3CN, 303 K, δ (ppm)): 76.6 (d, $^1J_{PH}$ = 459 Hz, $[HPCy_3]^+$).

Reaction of 4 with $[Cu(CH_3CN)_4]PF_6$ and PCy_3. In the drybox, 29 mg (0.078 mmol) of $[Cu(CH_3CN)_4]PF_6$ and 22 mg (0.078 mmol) of PCy_3 were dissolved in 5 mL of CH_3CN. An 80-mg (0.079-mmol) portion of **4b** was separately dissolved in 3 mL of CH_3CN. The latter was added to the former. A dark green precipitate formed immediately. The mixture was filtered, and the precipitate was washed with fresh CH_3CN three times and dried under vacuum. The infrared spectrum of the precipitate in THF confirmed that it was **1**, yield 45 mg, 56%. **4a** reacts similarly with $[Cu(CH_3CN)_4]PF_6$ and PCy_3.

Reaction of 4a with $HBF_4{\cdot}OEt_2$ or HCl. In the drybox, 120 mg (0.166 mmol) of **4a** was dissolved in 15 mL of Et_2O in a flask. A 27-mg (0.167-mmol) amount of $HBF_4{\cdot}OEt_2$ was diluted with 5 mL of Et_2O and was added dropwise to the former while it was stirred. A dark green solution was obtained. The flask was attached to an extractor and brought out of the drybox. Et_2O was removed under vacuum, and 5 mL of dry CH_3CN was condensed onto the residue at −78 °C. It was warmed to room temperature, and the mixture was filtered. A dark green precipitate was collected on the frit. It was washed with fresh CH_3CN again and dried under vacuum. Its IR and NMR spectra confirmed that it was **1**, yield 40 mg, 47%.

In a separate experiment, 40 mg (0.055 mmol) of **4a** was placed in a NMR tube, which was then attached to a vacuum adapter. An appropriate amount of THF-d_8 was condensed into the tube at −78 °C. Then 0.055 mmol of HCl, measured as the gas, was condensed into the tube at −195 °C. The NMR tube was then flame-sealed, and it was kept at −195 °C until NMR experiments were conducted. At −80 °C, two phosphorus resonances corresponding to **1** and **4a** were observed (δ 16.66 and 14.56 ppm) and there were two proton resonances at δ −5.80 and −15.00 ppm in the hydride region. When the tube was warmed to room temperature, **1** was the only phosphorus-containing species observed (δ 16.60 ppm) and there was only one proton signal at δ −14.83 ppm in the hydride region. The proton signal seemed to be associated with a hydridocarbonyliron compound, since no new phosphorus resonances were observed at either low or room temperature.

Results and Discussion

Syntheses: General Considerations. The vast majority of $M'(PR_3)$-containing complexes are synthesized by treating an anionic mono-, di-, or polynuclear precursor with the complexes $[M'X(PR_3)]$ (X = Cl, Br, I).[7] A modified and improved synthetic route by Salter and coworkers[7] involves the treatment of an anionic precursor with $[M'(CH_3CN)_4][PF_6]$ (M′ = Cu, Ag) at low temperature in solution, followed by the subsequent addition of an appropriate phosphine ligand to obtain the desired $M'(PR_3)$-containing cluster. We find that this synthetic method can be further modified under certain circumstances and reactions can be conducted at room temperature. A CH_3CN solution containing equimolar amounts of $[Cu(CH_3CN)_4][PF_6]$ (or $AgBF_4$) and free PR_3 can serve as the source of $[M'(PR_3)]^+$. Presumably, $[M'(PR_3)(CH_3CN)_x]^+$ is formed upon mixing of $[Cu(CH_3CN)_4]PF_6$ (or $AgBF_4$) and PR_3 in CH_3CN solution; $[M'(PR_3)(CH_3CN)_x]^+$ then loses labile CH_3CN ligands and undergoes electrophilic attack on an anionic precursor.

Syntheses of $M_2(CO)_8(\mu\text{-}M'PCy_3)_2$ (M = Fe, M′ = Cu (1); M = Fe, M′ = Ag (2); M = Ru, M′ = Cu (3)). The tetranuclear clusters $M_2(CO)_8(\mu\text{-}M'PCy_3)_2$ (M = Fe, M′ = Cu (**1**); M = Fe, M′ = Ag (**2**), M = Ru, M′ = Cu (**3**)) are prepared in 60–80% yields at room temperature when $[PPh_4]_2[M_2(CO)_8]$ (M = Fe, Ru) reacts with 2 equiv of $[Cu(CH_3CN)_4]PF_6$ (or $AgBF_4$) and 2 equiv of PCy_3 in CH_3CN solution according to eqs 1 and 2.

$$[PPh_4]_2[M_2(CO)_8] + 2[Cu(CH_3CN)_4]PF_6 + 2PCy_3 \xrightarrow{\text{M = Fe, Ru}} \underset{\text{M = Fe, 1; M = Ru, 3}}{(CO)_4M(\mu\text{-}Cu(PCy_3))_2M(CO)_4} \quad (1)$$

$$[PPh_4]_2[Fe_2(CO)_8] + 2AgBF_4 + 2PCy_3 \longrightarrow \underset{\mathbf{2}}{(CO)_4Fe(\mu\text{-}Ag(PCy_3))_2Fe(CO)_4} \quad (2)$$

1 can also be prepared in comparable yield from $Na_2[Fe_2(CO)_8]$; however, use of $Na_2[Fe_2(CO)_8]$ in the preparation of **2** also yields some unidentified side products that make the isolation of **2** difficult. $Na_2[Ru_2(CO)_8]$ is not used to prepare **3** simply because we have not been able to prepare a pure sample of $Na_2[Ru_2(CO)_8]$.[4] **1**, **2**, and **3** are dark green, green, and orange solids, respectively. All three solids are stable in air for more than 1 week. They are soluble in THF, toluene, CH_2Cl_2, and hexane.

Syntheses of $X[M_2(CO)_8(\mu\text{-}M'PCy_3)]$ (X = Na, M = Fe, M′ = Cu (4a); X = PPh_4, M = Fe, M′ = Cu (4b); X = PPh_4, M = Fe, M′ = Ag (5); X = PPh_4, M = Ru, M′ = Cu (6)). The trinuclear clusters $X[M_2(CO)_8(\mu\text{-}M'PCy_3)]$ (X = Na, M = Fe, M′ = Cu (**4a**); X = PPh_4, M = Fe, M′ = Cu (**4b**); X = PPh_4, M = Fe, M′ = Ag (**5**); X = PPh_4, M = Ru, M′ = Cu (**6**)) are synthesized when a CH_3CN solution containing equimolar amounts of $[Cu(CH_3CN)_4]PF_6$ (or $AgBF_4$) and PCy_3 is added to a CH_3CN solution containing 10–20% excess of $[M_2(CO)_8]^{2-}$ (eqs 3 and 4). Excess $[M_2(CO)_8]^{2-}$ avoids the production of neutral

$$X_2[M_2(CO)_8] + [Cu(CH_3CN)_4]PF_6 + PCy_3 \xrightarrow{\text{X = Na, PPh}_4;\ \text{M = Fe, Ru}} \left[(CO)_4M(\mu\text{-}Cu(PCy_3))M(CO)_4\right]^- X^+ \quad (3)$$

X = Na, M = Fe, **4a**
X = PPh_4, M = Fe, **4b**
X = PPh_4, M = Ru, **6**

$$[PPh_4]_2[Fe_2(CO)_8] + AgBF_4 + PCy_3 \longrightarrow \left[(CO)_4Fe(\mu\text{-}Ag(PCy_3))Fe(CO)_4\right]^- [PPh_4]^+ \quad (4)$$

5

tetranuclear clusters and is excluded from the product by solubility differences. Yields are between 80 and 100% for **4a,b** and **5**, but the yield is only about 60% for **6**. The low yield for **6** is due to the ready formation of the tetranuclear cluster **3** even in the presence of a large excess of $[Ru_2(CO)_8]^{2-}$.

4a,b are brown solids, **5** is a yellow solid, and **6** is an orange solid. Solid **4a** contains 0.5 CH_3CN solvent molecule per formula unit of **4a**, as shown by the elemental analysis and ^1H and ^{13}C NMR spectra. All of these clusters are extremely air-sensitive but can be stored in a drybox for weeks without apparent decomposition. They are soluble in CH_3CN, THF, and pyridine. The sodium salt of **4** (**4a**) is also soluble in Et_2O.

Synthesis of $[PPh_4]_2[[Fe_2(CO)_8]_2[\mu_4\text{-}\eta^2\text{-}Cu_2$-

($Cy_2PCH_2CH_2PCy_2$)]} (7). The hexanuclear complex $[PPh_4]_2\{[Fe_2(CO)_8]_2[\mu_4\text{-}\eta^2\text{-}Cu_2(Cy_2PCH_2CH_2PCy_2)]\}$ (7) is prepared with the diphos ligand $Cy_2PC_2CH_2PCy_2$ according to eq 5. In order to isolate 7, the CH_3CN solution

$$2[PPh_4]_2[Fe_2(CO)_8] + 2[Cu(CH_3CN)_4]PF_6 + (Cy)_2PCH_2CH_2P(Cy)_2 \longrightarrow \text{7} + 2[PPh_4]^+ \quad (5)$$

7

containing appropriate amounts of $[Cu(CH_3CN)_4][PF_6]$ and $Cy_2PCH_2CH_2PCy_2$ has to be added to the CH_3CN solution of $[PPh_4]_2[Fe_2(CO)_8]$. The color, solubility, and infrared spectrum of 7 are similar to those of **4b**.

Infrared and NMR Spectra. Infrared and NMR spectra of all the compounds are reported in the Experimental Section. Infrared spectra of **1–3** in the carbonyl stretching region show no absorptions below 1920 cm^{-1}, suggesting that all carbonyls in **1–3** are in terminal positions. The infrared absorptions of anionic species **4–7** in the carbonyl stretching region appear at lower energy than those of the neutral clusters **1–3**. Weak absorptions at 1730–1770 cm^{-1} in their infrared spectra are indicative of bridging carbonyls. The infrared spectra of **4b**, **5**, and **7** are similar to those reported for $[PPN][HFe_2(CO)_8]$[3e] and $[NEt_4][Fe_2(CO)_8(\mu\text{-}M'PPh_3)]$ (M′ = Cu, Au).[11]

In $^{31}P\{^1H\}$ NMR spectra, a singlet due to the phosphine ligand is observed for each of the Fe–Cu, Ru–Cu complexes **1**, **3**, **4**, **6**, and **7**; in the Fe–Ag complexes **2** and **5**, two doublets of approximately equal intensity are observed for each of these two compounds due to the couplings between ^{31}P and ^{109}Ag, ^{107}Ag nuclei. In the carbonyl region of $^{13}C\{^1H\}$ NMR spectra, a triplet is observed at δ 214.29 ppm ($^3J_{PC}$ = 2.3 Hz) for **1** and at δ 207.08 ppm ($^3J_{PC}$ = 2.3 Hz) for **3**. The observed triplets indicate that the Fe–Fe and Ru–Ru bonds are doubly bridged by two $Cu(PCy_3)$ fragments, thereby ruling out four-metal-chain Cu–Fe–Fe–Cu and Cu–Ru–Ru–Cu arrangements. For the $Cu(PCy_3)$ monobridged anions, there is a doublet ^{13}C resonance at δ 224.45 ppm ($^3J_{PC}$ = 1.8 Hz) for **4a**, δ 221.73 ppm ($^3J_{PC}$ = 1.9 Hz) for **4b**, and δ 212.20 ($^3J_{PC}$ = 2.3 Hz) for **6**. A resonance at δ 221.98 ppm is observed for **7**; the ^{13}C–^{31}P coupling is not resolved in this case.

Structures: General Comments. The $M'(PR_3)$ (M′ = Cu, Ag, Au) moiety can bridge a metal–metal bond or cap a triangular three-metal face in a polynuclear cluster.[7] Extended Hückel molecular orbital calculations by Evans and Mingos[12] have shown that the bonding characteristics of the $M'(PR_3)$ moiety are primarily determined by the hybrid s–p_z orbital (a_1 symmetry) and a higher lying pair of p_x and p_y orbitals (e symmetry). When a $M'(PR_3)$ group bridges a metal–metal bond, it utilizes its a_1 hybrid (s–p_z) orbital in a three-center two-electron interaction. In cases where the e set of p_x and p_y orbitals is too high in energy (e.g., in $Au(PH_3)$),[12] they do not provide any effective contribution to the bonding. In $Cu(PH_3)$, however, the role of the e orbitals is less clear. According to Evans and Mingos,[12] the empty and relatively low-lying p_x and p_y orbitals of the $Cu(PH_3)$ fragment may accept the back-donation of some electron density. In contrast, Braunstein and co-workers[13] find that the e orbitals are not significantly lower in energy in $Cu(PH_3)$ than in $Au(PH_3)$. In comparison with $Cu(PH_3)$, the more electron-donating phoshine PCy_3 would cause a raising of the p_x and p_y orbitals in $Cu(PCy_3)$, and therefore, we anticipate that only the hybrid s–p_z orbital of the $Cu(PCy_3)$ moiety would play a major role in the bonding.

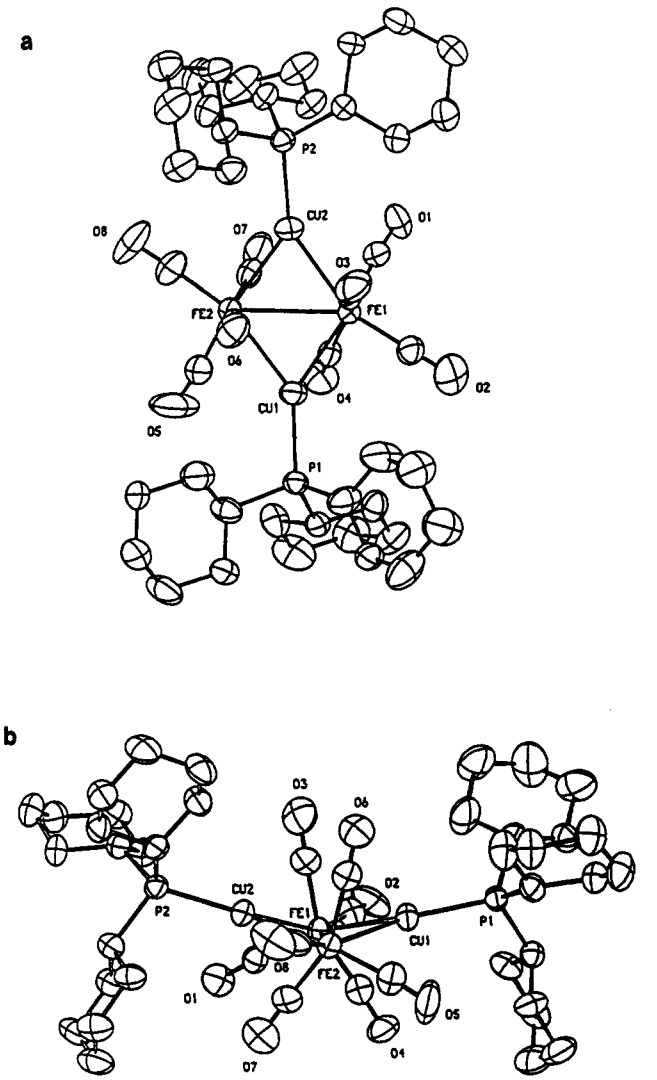

Figure 1. Two different views (top, a; bottom, b) of the molecular structure of $Fe_2(CO)_8(\mu\text{-}CuPCy_3)_2$ (1) showing the thermal ellipsoids at the 30% probability level. Hydrogen atoms are omitted.

In the trinuclear cluster anions **4–6** and in the hexanuclear complex **7**, each $M'(PR_3)$ fragment bridges the $M_2(CO)_8$ unit in a straightforward three-center two-electron interaction. In the neutral tetranuclear clusters **1–3**, two $M'(PCy_3)$ fragments bridge a formally *single* Fe–Fe or Ru–Ru bond. To our knowledge, no other simple metal–metal single bonds have been observed to be doubly bridged by two $M'(PR_3)$ fragments.[19] On the other hand, doubly protonated or doubly $Au(PEt_3)$ bridged metal–metal double-bond systems are known in the following compounds: $(\mu\text{-}H)_2Re_2(CO)_8$,[14] $[(\mu\text{-}H)_2W_2(CO)_8]^{2-}$,[15] $(\mu\text{-}H)_2Os_3(CO)_{10}$,[16] $Os_3(CO)_{10}(\mu\text{-}AuPEt_3)_2$,[17] and $[Mn_2(CO)_6\{\mu\text{-}(EtO)_2POP(OEt)_2\}(\mu\text{-}M'PPh_3)_2]$ (M′ = Cu, Ag, Au).[18] The uniqueness of the doubly bridged metal–metal single bonds observed in **1–3** deserves a careful examination of their molecular and electronic structures.

Structures of $Fe_2(CO)_8(\mu\text{-}CuPCy_3)_2$ (1) and $Ru_2(CO)_8(\mu\text{-}CuPCy_3)_2$ (3). The crystal structure of **1** and **3** are isomorphous with each other. Crystal data are in Table I. Positional parameters are listed in Tables II and III, respectively, and selected bond distances and bond angles are in Table IV. Figure 1 shows two views of the molecular structure of **1**. The molecular structure of **3** is shown in

Table II. Positional Parameters and Their Estimated Standard Deviations for $Fe_2(CO)_8[\mu\text{-}Cu(PCy_3)]_2$ (1)[a]

atom	x	y	z	B, Å²
Cu1	0.78578 (6)	0.02668 (4)	0.29211 (2)	3.25 (1)
Cu2	0.74308 (6)	0.14404 (4)	0.43012 (2)	3.30 (1)
Fe1	0.86965 (6)	0.03831 (4)	0.38563 (3)	2.71 (1)
Fe2	0.74877 (7)	0.16392 (4)	0.33123 (3)	2.85 (2)
P1	0.7667 (1)	−0.04944 (8)	0.21993 (5)	2.83 (3)
P2	0.6669 (1)	0.19501 (8)	0.50381 (5)	2.75 (3)
O1	1.0160 (4)	0.0887 (2)	0.4807 (2)	4.8 (1)
O2	0.9506 (4)	−0.1212 (2)	0.3830 (2)	6.2 (1)
O3	0.6386 (4)	−0.0237 (3)	0.4206 (2)	6.1 (1)
O4	1.0466 (3)	0.0851 (2)	0.3063 (2)	4.9 (1)
O5	0.8114 (5)	0.1883 (3)	0.2191 (2)	8.7 (1)
O6	0.5264 (3)	0.0709 (2)	0.3264 (2)	5.5 (1)
O7	0.9575 (4)	0.2400 (2)	0.3854 (2)	5.5 (1)
O8	0.6031 (4)	0.3013 (2)	0.3436 (2)	7.4 (1)
C1	0.9528 (5)	0.0721 (3)	0.4448 (2)	3.4 (1)
C2	0.9187 (5)	−0.0588 (3)	0.3834 (2)	3.9 (1)
C3	0.7264 (5)	0.0044 (3)	0.4074 (2)	3.8 (1)
C4	0.9720 (5)	0.0680 (3)	0.3351 (2)	3.6 (1)
C5	0.7877 (6)	0.1736 (3)	0.2624 (2)	4.5 (1)
C6	0.6165 (5)	0.1045 (3)	0.3285 (2)	3.8 (1)
C7	0.8768 (5)	0.2070 (3)	0.3655 (2)	3.7 (1)
C8	0.6615 (5)	0.2473 (3)	0.3400 (3)	4.4 (1)
C11	0.6633 (5)	−0.0105 (3)	0.1661 (2)	3.9 (1)
C12	0.6520 (5)	−0.0579 (3)	0.1138 (2)	4.0 (1)
C13	0.5678 (5)	−0.0189 (4)	0.0715 (2)	5.7 (2)
C14	0.4533 (6)	0.0095 (4)	0.0919 (2)	5.6 (2)
C15	0.4715 (6)	0.0583 (3)	0.1414 (2)	4.9 (1)
C16	0.5453 (6)	0.0168 (4)	0.1855 (3)	5.9 (2)
C21	0.7098 (6)	−0.1483 (3)	0.2334 (2)	5.0 (1)
C22	0.7506 (5)	−0.2120 (3)	0.1973 (2)	4.0 (1)
C23	0.6938 (6)	−0.2899 (4)	0.2081 (3)	6.6 (2)
C24	0.6898 (9)	−0.3093 (4)	0.2642 (3)	8.7 (2)
C25	0.6435 (7)	−0.2451 (4)	0.3004 (3)	7.1 (2)
C26	0.7031 (8)	−0.1688 (4)	0.2899 (3)	7.4 (2)
C31	0.9143 (5)	−0.0624 (3)	0.1891 (2)	3.1 (1)
C32	1.0064 (5)	−0.0966 (3)	0.2302 (2)	4.0 (1)
C33	1.1290 (5)	−0.1063 (4)	0.2069 (3)	5.3 (2)
C34	1.1751 (5)	−0.0312 (4)	0.1860 (3)	5.7 (2)
C35	1.0870 (6)	0.0045 (5)	0.1445 (3)	6.3 (2)
C36	0.9622 (5)	0.0142 (3)	0.1677 (2)	4.2 (1)
C41	0.6542 (5)	0.1309 (3)	0.5634 (2)	3.1 (1)
C42	0.6631 (5)	0.1703 (3)	0.6187 (2)	3.7 (1)
C43	0.6369 (5)	0.1134 (4)	0.6633 (2)	4.6 (1)
C44	0.7243 (5)	0.0456 (4)	0.6626 (2)	4.5 (1)
C45	0.7210 (5)	0.0070 (3)	0.6077 (2)	4.3 (1)
C46	0.7416 (5)	0.0629 (3)	0.5621 (2)	3.7 (1)
C51	0.7559 (4)	0.2802 (3)	0.5262 (2)	3.1 (1)
C52	0.8889 (5)	0.2554 (3)	0.5374 (2)	4.0 (1)
C53	0.9669 (5)	0.3240 (3)	0.5559 (3)	4.9 (1)
C54	0.9601 (6)	0.3873 (4)	0.5140 (3)	5.5 (2)
C55	0.8311 (5)	0.4131 (3)	0.5028 (3)	4.8 (2)
C56	0.7495 (5)	0.3455 (3)	0.4848 (2)	3.9 (1)
C61	0.5118 (4)	0.2302 (3)	0.4891 (2)	3.1 (1)
C62	0.4489 (5)	0.2672 (3)	0.5366 (2)	4.2 (1)
C63	0.3214 (5)	0.2962 (4)	0.5200 (3)	4.7 (1)
C64	0.2458 (5)	0.2325 (4)	0.4953 (3)	5.2 (2)
C65	0.3061 (5)	0.1968 (4)	0.4472 (3)	4.8 (1)
C66	0.4336 (5)	0.1661 (3)	0.4633 (2)	4.1 (1)

[a] Anisotropically refined atoms are given in the form of the isotropic equivalent displacement parameter defined as $^4/_3[a^2\beta(1,1) + b^2\beta(2,2) + c^2\beta(3,3) + ab(\cos\gamma)\beta(1,2) + ac(\cos\beta)\beta(1,3) + bc(\cos\alpha)\beta(2,3)]$. Calculated hydrogen atom positional parameters are included in the supplementary material.

Table III. Positional Parameters and Their Estimated Standard Deviations for $Ru_2(CO)_8[\mu\text{-}Cu(PCy_3)]_2$ (3)[a]

atom	x	y	z	B, Å²
Ru1	0.12765 (2)	0.03703 (1)	0.11449 (1)	1.983 (5)
Ru2	0.25559 (2)	0.16762 (1)	0.17125 (1)	2.059 (5)
Cu1	0.21305 (4)	0.02698 (2)	0.21123 (2)	2.464 (8)
Cu2	0.25414 (4)	0.14915 (2)	0.06958 (2)	2.489 (8)
P1	0.23362 (7)	−0.04719 (5)	0.28308 (3)	2.09 (2)
P2	0.33057 (7)	0.19848 (5)	−0.00332 (3)	2.07 (2)
O1	−0.0224 (2)	0.0890 (2)	0.01522 (9)	3.82 (6)
O2	0.0516 (3)	−0.1299 (2)	0.1219 (1)	4.95 (7)
O3	0.3709 (2)	−0.0212 (2)	0.0746 (1)	4.80 (7)
O4	−0.0628 (2)	0.0876 (2)	0.1930 (1)	3.86 (6)
O5	0.2142 (4)	0.1888 (2)	0.2899 (1)	7.11 (9)
O6	0.4856 (2)	0.0662 (2)	0.1761 (1)	4.07 (6)
O7	0.0251 (2)	0.2458 (2)	0.1236 (1)	4.99 (7)
O8	0.4028 (3)	0.3103 (2)	0.1476 (1)	5.59 (7)
C1	0.0420 (3)	0.0738 (2)	0.0505 (1)	2.66 (7)
C2	0.0799 (3)	−0.0672 (2)	0.1204 (1)	3.12 (8)
C3	0.2820 (3)	0.0031 (2)	0.0887 (1)	3.06 (7)
C4	0.0109 (3)	0.0700 (2)	0.1644 (1)	2.74 (7)
C5	0.2259 (4)	0.1746 (2)	0.2460 (1)	3.91 (9)
C6	0.3984 (3)	0.1025 (2)	0.1752 (1)	2.82 (7)
C7	0.1097 (3)	0.2147 (2)	0.1417 (2)	3.34 (8)
C8	0.3470 (3)	0.2560 (2)	0.1545 (2)	3.48 (8)
C11	0.2978 (3)	−0.1448 (2)	0.2717 (1)	3.08 (7)
C12	0.2503 (3)	−0.2097 (2)	0.3052 (1)	3.03 (7)
C13	0.3135 (4)	−0.2852 (2)	0.2958 (2)	4.14 (9)
C14	0.3153 (5)	−0.3067 (3)	0.2391 (2)	5.6 (1)
C15	0.3640 (4)	−0.2419 (3)	0.2046 (2)	5.2 (1)
C16	0.3001 (4)	−0.1662 (2)	0.2141 (2)	4.9 (1)
C21	0.3339 (3)	−0.0058 (2)	0.3373 (1)	2.70 (7)
C22	0.4550 (3)	0.0195 (2)	0.3167 (1)	3.26 (8)
C23	0.5311 (3)	0.0613 (2)	0.3598 (1)	3.14 (8)
C24	0.5514 (3)	0.0111 (2)	0.4090 (1)	3.50 (8)
C25	0.4322 (3)	−0.0144 (2)	0.4300 (1)	3.79 (9)
C26	0.3506 (3)	−0.0549 (2)	0.3875 (1)	2.87 (7)
C31	0.0828 (3)	−0.0608 (2)	0.3120 (1)	2.47 (7)
C32	0.0352 (3)	0.0152 (2)	0.3331 (2)	3.58 (8)
C33	−0.0925 (4)	0.0061 (3)	0.3535 (2)	4.6 (1)
C34	−0.1795 (3)	−0.0265 (3)	0.3108 (2)	4.19 (9)
C35	−0.1340 (3)	−0.1017 (2)	0.2907 (2)	3.64 (8)
C36	−0.0064 (3)	−0.0936 (2)	0.2695 (1)	2.84 (7)
C41	0.4878 (3)	0.2334 (2)	0.0114 (1)	2.37 (7)
C42	0.5659 (3)	0.1692 (2)	0.0373 (1)	3.00 (7)
C43	0.6923 (3)	0.1993 (2)	0.0536 (2)	3.67 (8)
C44	0.7555 (3)	0.2337 (2)	0.0069 (2)	3.97 (9)
C45	0.6790 (3)	0.2977 (2)	−0.0187 (2)	3.58 (8)
C46	0.5512 (3)	0.2692 (2)	−0.0355 (1)	3.01 (7)
C51	0.3433 (3)	0.1347 (2)	−0.0618 (1)	2.28 (6)
C52	0.3338 (3)	0.1739 (2)	−0.1166 (1)	2.87 (7)
C53	0.3610 (3)	0.1159 (2)	−0.1605 (1)	3.31 (8)
C54	0.2724 (3)	0.0479 (2)	−0.1594 (1)	3.22 (8)
C55	0.2786 (3)	0.0089 (2)	−0.1050 (1)	3.16 (8)
C56	0.2556 (3)	0.0662 (2)	−0.0608 (1)	2.68 (7)
C61	0.2408 (3)	0.2828 (2)	−0.0264 (1)	2.41 (7)
C62	0.1077 (3)	0.2582 (2)	−0.0366 (1)	2.99 (7)
C63	0.0284 (3)	0.3258 (2)	−0.0552 (2)	3.69 (8)
C64	0.0344 (3)	0.3898 (2)	−0.0147 (2)	4.23 (9)
C56	0.1638 (3)	0.4157 (2)	−0.0037 (2)	3.65 (8)
C66	0.2467 (3)	0.3488 (2)	0.0143 (1)	3.12 (8)

[a] See footnote *a* of Table II.

Figure 2, and it is nearly identical with that of 1.

In both structures, a $M_2(CO)_8$ unit is bridged by two $Cu(PCy_3)$ fragments. The M_2Cu_2 metal cores are of the butterfly type. The dihedral angles between two CuM_2 lanes are 148.3 and 151.6° for 1 and 3, respectively. The molecules have *pseudo*-C_2 symmetry; the 2-fold axis passes through the midpoint of the M–M bond and bisects the dihedral angle.

Each Cu atom in both structures lies in the plane defined by two M atoms and the ligated P atom. This is expected since the $Cu(PCy_3)$ fragments bridge M–M bonds by utilizing the s–p_z hybridized orbitals. The carbonyl groups and the Cu atoms are arranged as a highly distorted octahedron around each M atom. For example (see Figure 1b), Fe2 has C6–O6 and C7–O7 in the axial positions and has C5–O5, C8–O8, and the Cu2 atom in the equatorial positions; because of the butterfly nature of the Fe_2Cu_2 core, the Cu1 atom is out of the plane defined by the equatorial carbonyls C5O5 and C8O8. On the other hand, Cu1, C1–O1, and C2–O2 are in the equatorial positions of the Fe1 octahedron with Cu2 out of the equatorial plane. The maximum deviation of the angles from the ideal octahedral geometry is about 30°, the same magnitude as the

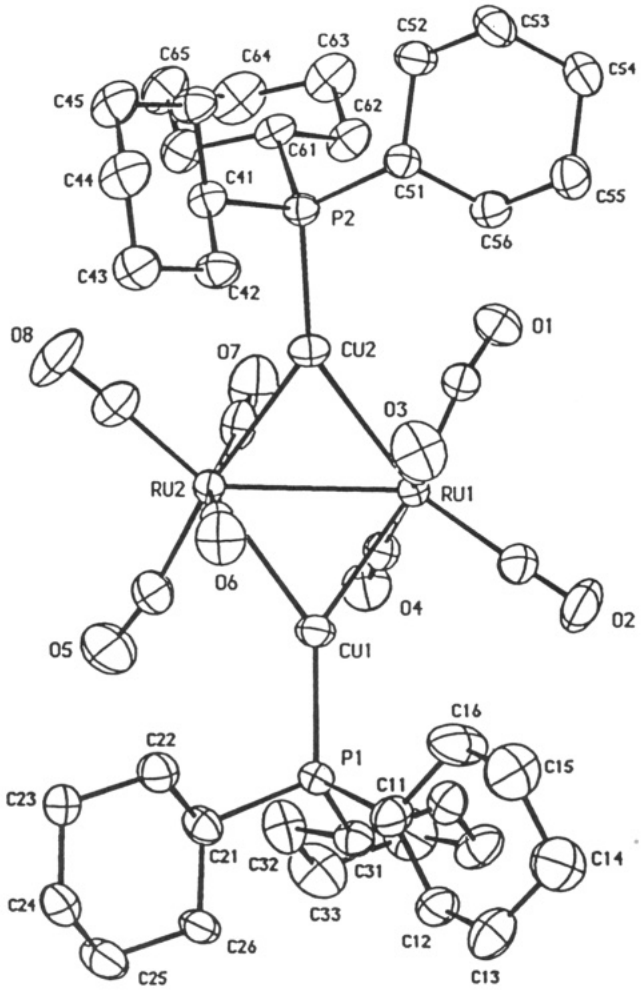

Figure 2. Molecular structure of $Ru_2(CO)_8(\mu\text{-}CuPCy_3)_2$ (**3**) showing the thermal ellipsoids at the 30% probability level. Hydrogen atoms are omitted.

dihedral angles. All carbonyls in both structures are essentially linear.

The Fe–Fe distance in **1** is 2.862 (1) Å, 0.07 Å longer than that of its parent compound $Fe_2(CO)_8^{2-}$ (2.792 (1) Å).[4b] Similarly, the Ru–Ru distance of 2.9990 (3) Å in **3** is 0.06 Å longer than that in $Ru_2(CO)_8^{2-}$ (2.936 (1) Å).[4] These are considered to be Fe–Fe and Ru–Ru single-bond distances. In both structures, each Cu atom is bonded to the M–M bond in an asymmetric fashion: in **1**, the Cu1–Fe1 distance is 2.4726 (9) Å, significantly shorter than the Cu1–Fe2 distance of 2.6063 (9) Å, while the Cu2–Fe2 distance of 2.4822 (9) Å is much shorter than the Cu2–Fe1 distance of 2.5791 (9) Å. The metal–metal distances in **3** are Cu1–Ru1 = 2.5770 (4) Å, Cu1–Ru2 = 2.6911 (4) Å, Cu2–Ru1 = 2.6740 (4) Å, and Cu2–Ru2 = 2.5782 (4) Å. The differences are on the order of 0.1 Å. It is hard to distinguish between steric effects and electronic effects as the cause of this distortion. However, we do not note any short intermolecular contacts which would imply steric problems (the closest intermolecular contacts are 3.241 (9) and 3.230 (5) Å, respectively, for **1** and **3**, between two O1 atoms from different molecules). As far as the electronic effects are concerned, we offer a qualitative explanation in terms of the second-order Jahn–Teller effect[8] as described below.

Structural Distortions in 1 and 3. The solid-state structures of **1** and **3** have pseudo-C_2 symmetry. In principle, they can be derived from two-step distortions of a D_{2h} metal core (Chart I; the axial carbonyl groups are omitted for clarity). The first step involves distortion of

Chart I

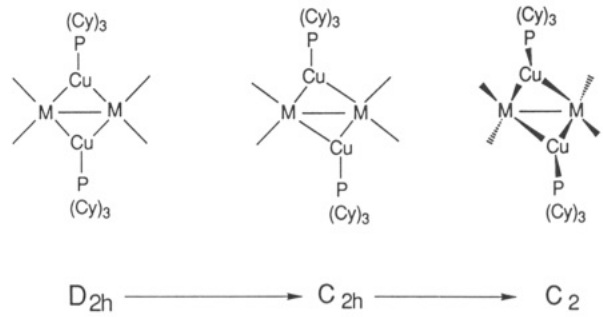

Chart II

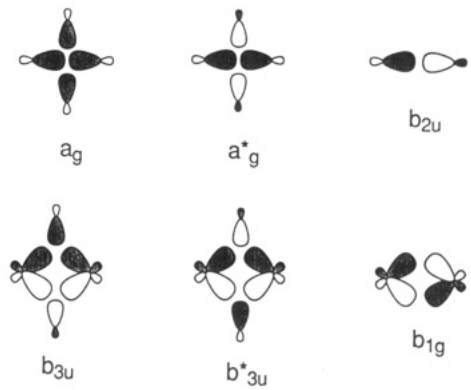

the M_2Cu_2 metal core from a rhombus to a parallelogram with two long peripheral edges and two short ones, thus reducing the symmetry from D_{2h} to C_{2h}. In the second step, the M_2Cu_2 metal core is puckered along the M–M vector by about 30°, causing the carbonyls to tilt accordingly. The symmetry is further lowered from C_{2h} to C_2.

A second-order Jahn–Teller effect[8] might be responsible for the first step in the distortion process. Employing the Fenske–Hall MO method, Cotton and Fang[20] showed that the metal–metal bond distortion in $W_4(OEt)_{16}$ is "a clear and affirmative example of the second-order Jahn–Teller effect". The bond distortions in several other cluster compounds were explained similarly.[21] We apply the same concept to compounds **1** and **3** in terms of frontier orbital interactions. The $Fe_2(CO)_8$ fragment with D_{2h} point symmetry is isolobal with the ethylene molecule.[22] Each Cu(PCy$_3$) fragment has an s–p$_z$ hybridized orbital which may participate in the bonding. Chart II shows the interactions of the frontier orbitals from one $Fe_2(CO)_8$ and two Cu(PCy$_3$) units.

This formalism follows the bonding picture of the hydrogen bridge system of diborane by Longuet-Higgins.[23] Similar orbital interactions were also sketched by Broach and Williams[16b] to interpret the H_2Os_2 bonding in $(\mu\text{-}H)_2Os_3(CO)_{10}$. According to this bonding picture, four valence electrons are associated with the H_2M_2 or M_2Au_2 cores in the doubly protonated or doubly Au(PEt$_3$) bridged double-bond systems, such as $[(\mu\text{-}H)_2W_2(CO)_8]^{2-}$,[15] $(\mu\text{-}H)_2Os_3(CO)_{10}$,[16] and $Os_3(CO)_{10}(\mu\text{-}AuPEt_3)_2$.[17] These electrons occupy two bonding orbitals, a_g and b_{3u} (D_{2h} point group for $[(\mu\text{-}H)_2W_2(CO)_8]^{2-}$) or a_g and b_u (C_{2v} point group for $(\mu\text{-}H)_2Os_3(CO)_{10}$ and $Os_3(CO)_{10}(\mu\text{-}AuPEt_3)_2$), thus leading to the formal double bonds and symmetrical bridging. In the Fe_2Cu_2 and Ru_2Cu_2 metal cores reported here, however, there are six valence electrons associated with each core. Four electrons fill the two bonding orbitals a_g and b_{3u}. The extra two electrons should occupy the lowest of the remaining four orbitals (a^*_g, b^*_{3u}, b_{2u}, and b_{1g}). The observed distortion of the metal core can be

Table IV. Selected Bond Distances (Å) and Angles (deg) for $Fe_2(CO)_8(\mu\text{-}CuPCy_3)_2$ (1) and $Ru_2(CO)_8(\mu\text{-}CuPCy_3)_2$ (3)

1		3		1		3	
			Distances				
Fe1-Fe2	2.862 (1)	Ru1-Ru2	2.9990 (3)	O1-C1	1.145 (7)	O1-C1	1.143 (3)
Fe1-Cu1	2.4726 (9)	Ru1-Cu1	2.5770 (4)	O2-C2	1.137 (7)	O2-C2	1.133 (4)
Fe1-Cu2	2.5791 (9)	Ru1-Cu2	2.6740 (4)	O3-C3	1.144 (6)	O3-C3	1.137 (4)
Fe2-Cu1	2.6063 (9)	Ru2-Cu1	2.6911 (4)	O4-C4	1.151 (6)	O4-C4	1.150 (3)
Fe2-Cu2	2.4822 (9)	Ru2-Cu2	2.5782 (4)	O5-C5	1.144 (7)	O5-C5	1.145 (4)
Cu1-P1	2.228 (1)	Cu1-P1	2.2238 (8)	O6-C6	1.152 (8)	O6-C6	1.148 (4)
Cu2-P2	2.227 (1)	Cu2-P2	2.2238 (8)	O7-C7	1.153 (8)	O7-C7	1.153 (5)
Fe1-C1	1.798 (6)	Ru1-C1	1.939 (3)	O8-C8	1.142 (9)	O8-C8	1.144 (4)
Fe1-C2	1.769 (6)	Ru1-C2	1.893 (3)	P1-C11	1.850 (5)	P1-C11	1.864 (3)
Fe1-C3	1.792 (6)	Ru1-C3	1.938 (3)	P1-C21	1.860 (6)	P1-C21	1.862 (3)
Fe1-C4	1.797 (5)	Ru1-C4	1.926 (3)	P1-C31	1.842 (5)	P1-C31	1.857 (3)
Fe2-C5	1.787 (5)	Ru2-C5	1.927 (3)	P2-C41	1.859 (5)	P2-C41	1.857 (3)
Fe2-C6	1.786 (6)	Ru2-C6	1.936 (3)	P2-C51	1.846 (5)	P2-C51	1.853 (3)
Fe2-C7	1.784 (6)	Ru2-C7	1.923 (3)	P2-C61	1.841 (5)	P2-C61	1.847 (3)
Fe2-C8	1.754 (6)	Ru2-C8	1.893 (3)				
			Angles				
Fe2-Fe1-Cu1	57.94 (3)	Ru2-Ru1-Cu1	57.11 (1)	Cu2-Fe2-C7	68.7 (2)	Cu2-Ru2-C7	72.56 (9)
Fe2-Fe1-Cu2	53.98 (2)	Ru2-Ru1-Cu2	53.69 (1)	Cu2-Fe2-C8	87.4 (2)	Cu2-Ru2-C8	82.01 (1)
Fe2-Fe1-C1	110.6 (2)	Ru2-Ru1-C1	110.32 (8)	C5-Fe2-C6	104.2 (3)	C5-Ru2-C6	99.2 (1)
Fe2-Fe1-C2	147.7 (2)	Ru2-Ru1-C2	114.35 (9)	C5-Fe2-C7	101.6 (3)	C5-Ru2-C7	100.1 (1)
Fe2-Fe1-C3	89.5 (2)	Ru2-Ru1-C3	89.36 (9)	C5-Fe2-C8	101.3 (3)	C5-Ru2-C8	106.3 (1)
Fe2-Fe1-C4	75.4 (2)	Ru2-Ru1-C4	77.12 (8)	C6-Fe2-C7	152.9 (3)	C6-Ru2-C7	158.6 (1)
Cu1-Fe1-Cu2	105.73 (3)	Cu1-Ru1-Cu2	105.87 (1)	C6-Fe2-C8	91.5 (3)	C6-Ru2-C8	92.7 (1)
Cu1-Fe1-C1	162.4 (2)	Cu1-Ru1-C1	162.01 (8)	C7-Fe2-C8	91.4 (3)	C7-Ru2-C8	90.7 (1)
Cu1-Fe1-C2	89.8 (2)	Cu1-Ru1-C2	87.28 (9)	Fe1-Cu1-Fe2	68.55 (3)	Ru1-Cu1-Ru2	69.36 (1)
Cu1-Fe1-C3	87.4 (2)	Cu1-Ru1-C3	90.41 (9)	Fe1-Cu1-P1	145.39 (5)	Ru1-Cu1-P1	145.83 (3)
Cu1-Fe1-C4	65.8 (2)	Cu1-Ru1-C4	68.28 (8)	Fe2-Cu1-P1	145.93 (5)	Ru2-Cu1-P1	144.77 (2)
Cu2-Fe1-C1	71.8 (2)	Cu2-Ru1-C1	69.63 (8)	Fe1-Cu2-Fe2	68.85 (3)	Ru1-Cu2-Ru2	69.61 (1)
Cu2-Fe1-C2	149.4 (2)	Cu2-Ru1-C2	151.8 (1)	Fe1-Cu2-P2	149.61 (5)	Ru1-Cu2-P2	148.50 (2)
Cu2-Fe1-C3	66.6 (2)	Cu2-Ru1-C3	66.33 (9)	Fe2-Cu2-P2	141.54 (5)	Ru2-Cu2-P2	141.71 (2)
Cu2-Fe1-C4	117.5 (2)	Cu2-Ru1-C4	115.75 (9)	Cu1-P1-C11	113.6 (2)	Cu1-P1-C11	115.3 (1)
C1-Fe1-C2	100.9 (3)	C1-Ru1-C2	104.7 (1)	Cu1-P1-C21	115.0 (2)	Cu1-P1-C21	114.1 (1)
C1-Fe1-C3	106.7 (3)	C1-Ru1-C3	102.9 (1)	Cu1-P1-C31	115.5 (2)	Cu1-P1-C31	109.34 (9)
C1-Fe1-C4	99.3 (3)	C1-Ru1-C4	97.4 (1)	C11-P1-C21	105.2 (3)	C11-P1-C21	104.3 (1)
C2-Fe1-C3	88.5 (2)	C2-Ru1-C3	89.2 (1)	C11-P1-C31	106.0 (2)	C11-P1-C31	107.2 (1)
C2-Fe1-C4	92.7 (2)	C2-Ru1-C4	92.2 (1)	C21-P1-C31	105.9 (3)	C21-P1-C31	105.9 (1)
C3-Fe1-C4	153.2 (3)	C3-Ru1-C4	158.5 (1)	Cu2-P2-C41	117.4 (2)	Cu2-P2-C41	110.17 (9)
Fe1-Fe2-Cu1	53.51 (2)	Ru1-Ru2-Cu1	53.53 (1)	Cu2-P2-C51	110.5 (2)	Cu2-P2-C51	117.99 (9)
Fe1-Fe2-Cu2	57.18 (2)	Ru1-Ru2-Cu2	56.70 (1)	Cu2-P2-C61	110.3 (2)	Cu2-P2-C61	110.39 (9)
Fe1-Fe2-C5	113.4 (2)	Ru1-Ru2-C5	114.6 (1)	C41-P2-C51	107.1 (2)	C41-P2-C51	104.6 (1)
Fe1-Fe2-C6	86.9 (2)	Ru1-Ru2-C6	86.91 (8)	C41-P2-C61	104.9 (2)	C41-P2-C61	106.6 (1)
Fe1-Fe2-C7	75.4 (2)	Ru1-Ru2-C7	76.75 (9)	C51-P2-C61	105.9 (2)	C51-P2-C61	106.4 (1)
Fe1-Fe2-C8	144.6 (2)	Ru1-Ru2-C8	138.7 (1)	Fe1-C1-O1	172.5 (6)	Ru1-C1-O1	169.8 (3)
Cu1-Fe2-Cu2	104.63 (3)	Cu1-Ru2-Cu2	105.34 (1)	Fe1-C2-O2	178.6 (5)	Ru1-C2-O2	177.4 (3)
Cu1-Fe2-C5	71.5 (2)	Cu1-Ru2-C5	69.7 (1)	Fe1-C3-O3	174.0 (5)	Ru1-C3-O3	175.8 (3)
Cu1-Fe2-C6	66.5 (2)	Cu1-Ru2-C6	66.75 (9)	Fe1-C4-O4	173.3 (6)	Ru1-C4-O4	176.9 (3)
Cu1-Fe2-C7	115.2 (2)	Cu1-Ru2-C7	112.02 (9)	Fe2-C5-O5	172.6 (5)	Ru2-C5-O5	170.7 (3)
Cu1-Fe2-C8	153.1 (2)	Cu1-Ru2-C8	157.26 (9)	Fe2-C6-O6	175.1 (5)	Ru2-C6-O6	177.0 (3)
Cu2-Fe2-C5	167.3 (2)	Cu2-Ru2-C5	169.3 (1)	Fe2-C7-O7	174.6 (6)	Ru2-C7-O7	177.1 (3)
Cu2-Fe2-C6	84.5 (2)	Cu2-Ru2-C6	86.98 (8)	Fe2-C8-O8	177.2 (6)	Ru2-C8-O8	176.0 (3)

accounted for by a second-order Jahn–Teller effect if the b_{1g} and a^*_g orbitals are close in energy and are the HOMO and LUMO (no matter which orbital is HOMO or LUMO). When the HOMO and LUMO are close in energy, they become pseudodegenerate and are subject to the second-order Jahn–Teller effect.[8] The mode of distortion in a symmetrical structure is governed by the symmetry rule: the distortion will take the form of one of the normal vibrations of the symmetrical molecule, and this vibration must belong to the same representation as the direct product of the electronic terms of the ground state and the excited state.[8,20] The normal modes of the M_2Cu_2 metal core are illustrated in Chart III.

With the assumption that b_{1g} and a^*_g are the HOMO and LUMO, the ground state is A_g (resulting from either $b_{1g} \times b_{1g}$ or $a^*_g \times a^*_g$), and the excited state is B_{1g} (from either $b_{1g} \times a^*_g$ or $a^*_g \times b_{1g}$). Since the direct product $A_g \times B_{1g}$ is B_{1g}, the distortion will take the form of a b_{1g} normal vibration shown in Chart III, which will lead to the distortion that is observed in 1 and 3. The distorted structure is stabilized by opening up an energy gap between the HOMO and LUMO.

Chart III

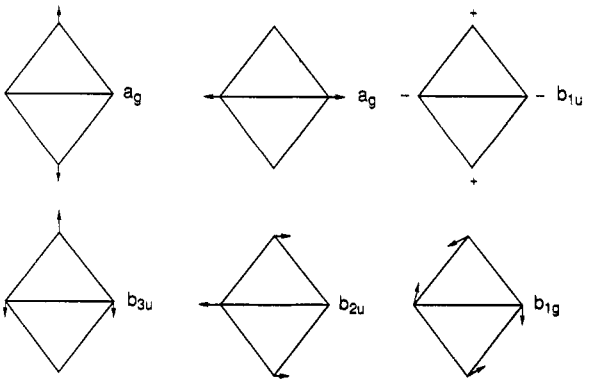

Step 2 of the distortion in Chart I is the puckering of the M_2Cu_2 metal core by 30°. Mingos and May[24] point out

Table V. Positional Parameters and Their Estimated Standard Deviations for $[PPh_4][Fe_2(CO)_8(\mu\text{-}CuPCy_3)]\cdot 0.5THF$ (4b·0.5THF)[a]

atom	x	y	z	B, Å²	atom	x	y	z	B, Å²
Cu	0.3047 (1)	0.1744 (2)	−0.22258 (6)	4.01 (4)	C35	0.085 (2)	−0.142 (2)	−0.0439 (9)	15.2 (7)
Fe1	0.2371 (2)	0.0602 (2)	−0.31983 (7)	3.80 (5)	C36	0.143 (1)	−0.002 (2)	−0.0570 (7)	7.9 (5)
Fe2	0.4892 (2)	0.2951 (2)	−0.27624 (7)	3.41 (4)	C41	−0.712 (1)	−0.4959 (9)	−0.4551 (5)	2.7 (3)
P1	0.2496 (3)	0.1760 (3)	−0.1389 (1)	4.13 (9)	C42	−0.719 (1)	−0.601 (1)	−0.4283 (5)	4.2 (4)
P2	−0.7008 (3)	−0.3601 (3)	−0.4151 (1)	3.04 (8)	C43	−0.725 (1)	−0.707 (1)	−0.4578 (6)	4.4 (3)
O1	−0.0142 (9)	−0.1645 (9)	−0.3736 (5)	7.5 (3)	C44	−0.723 (1)	−0.707 (1)	−0.5136 (6)	4.4 (3)
O2	0.0589 (9)	0.1941 (9)	−0.3376 (4)	7.0 (3)	C45	−0.714 (1)	−0.599 (1)	−0.5411 (5)	4.9 (4)
O3	0.3908 (8)	0.0623 (7)	−0.4083 (4)	5.0 (2)	C46	−0.710 (1)	−0.498 (1)	−0.5112 (5)	3.7 (3)
O4	0.288 (1)	−0.0846 (8)	−0.2269 (4)	8.6 (4)	C51	−0.8317 (9)	−0.4136 (9)	−0.3720 (5)	2.8 (3)
O5	0.594 (1)	0.1192 (9)	−0.2258 (5)	8.3 (4)	C52	−0.958 (1)	−0.521 (1)	−0.3906 (5)	3.6 (3)
O6	0.3127 (9)	0.4241 (8)	−0.2635 (5)	7.2 (3)	C53	−1.060 (1)	−0.556 (1)	−0.3604 (6)	5.0 (4)
O7	0.7249 (9)	0.508 (1)	−0.2044 (5)	8.0 (4)	C54	−1.040 (1)	−0.487 (1)	−0.3112 (5)	4.5 (3)
O8	0.5886 (8)	0.3538 (8)	−0.3830 (4)	5.3 (3)	C55	−0.914 (1)	−0.379 (1)	−0.2914 (5)	5.0 (4)
C1	0.086 (1)	−0.076 (1)	−0.3520 (6)	5.5 (4)	C56	−0.810 (1)	−0.343 (1)	−0.3218 (5)	4.5 (4)
C2	0.136 (1)	0.145 (1)	−0.3286 (5)	5.3 (4)	C61	−0.738 (1)	−0.2582 (9)	−0.4638 (5)	2.6 (3)
C3	0.336 (1)	0.068 (1)	−0.3720 (5)	3.7 (3)	C62	−0.642 (1)	−0.194 (1)	−0.4969 (5)	4.0 (3)
C4	0.271 (1)	−0.022 (1)	−0.2604 (6)	6.0 (5)	C63	−0.673 (1)	−0.119 (1)	−0.5366 (5)	4.2 (4)
C5	0.546 (1)	0.181 (1)	−0.2472 (6)	5.2 (4)	C64	−0.798 (1)	−0.104 (1)	−0.5407 (5)	3.8 (3)
C6	0.374 (1)	0.365 (1)	−0.2674 (6)	4.4 (4)	C65	−0.887 (1)	−0.164 (1)	−0.5070 (6)	4.8 (4)
C7	0.633 (1)	0.423 (1)	−0.2322 (6)	4.8 (4)	C66	−0.860 (1)	−0.243 (1)	−0.4688 (5)	3.5 (3)
C8	0.543 (1)	0.325 (1)	−0.3419 (6)	4.0 (3)	C71	−0.527 (1)	−0.275 (1)	−0.3716 (5)	3.1 (3)
C11	0.411 (1)	0.267 (2)	−0.0819 (5)	6.9 (4)	C72	−0.471 (1)	−0.145 (1)	−0.3597 (6)	4.9 (4)
C12	0.486 (1)	0.407 (2)	−0.0931 (6)	7.2 (5)	C73	−0.0336 (1)	−0.076 (1)	−0.3262 (7)	6.1 (5)
C13	0.625 (1)	0.482 (2)	−0.0486 (8)	11.4 (6)	C74	−0.257 (1)	−0.137 (1)	−0.3044 (6)	5.0 (4)
C14	0.721 (2)	0.418 (2)	−0.0483 (8)	14.3 (8)	C75	−0.310 (1)	−0.263 (1)	−0.3147 (7)	5.5 (4)
C15	0.648 (1)	0.278 (2)	−0.0370 (8)	12.4 (7)	C76	−0.446 (1)	−0.335 (1)	−0.3502 (5)	4.0 (3)
C16	0.511 (1)	0.201 (1)	−0.0815 (7)	7.8 (5)	O9	0.443	0.166	0.084	10 (1)*
C21	0.138 (1)	0.259 (1)	−0.1387 (5)	4.8 (4)	C81	0.557	0.250	0.127	11 (2)*
C22	0.033 (1)	0.234 (2)	−0.1872 (7)	13.1 (6)	C82	0.529	0.307	0.170	7 (2)*
C23	−0.039 (1)	0.319 (2)	−0.1926 (7)	10.4 (5)	C83	0.389	0.166	0.168	6 (1)*
C24	−0.085 (2)	0.330 (2)	−0.1417 (8)	12.8 (6)	C84	0.359	0.082	0.115	6 (1)*
C25	0.024 (1)	0.362 (1)	−0.0893 (7)	9.3 (5)	O10	0.473	0.250	0.179	13 (2)*
C26	0.103 (1)	0.282 (1)	−0.0842 (6)	6.3 (4)	C91	0.584	0.279	0.158	9 (2)*
C31	0.161 (1)	0.016 (1)	−0.1178 (6)	6.0 (4)	C92	0.529	0.279	0.105	6 (2)*
C32	0.036 (2)	−0.066 (2)	−0.1566 (8)	12.1 (8)	C93	0.389	0.166	0.104	12 (3)*
C33	−0.014 (2)	−0.206 (2)	−0.1445 (9)	11.9 (8)	C94	0.416	0.109	0.156	15 (3)*
C34	−0.030 (3)	−0.217 (2)	−0.084 (1)	17 (1)					

[a] See footnote *a* of Table II. The positions of the disordered THF molecule (starred values) were located from difference Fourier maps, and their multiplicities were assigned to 0.25. Their positions were fixed, and thermal parameters were refined isotropically.

that the potential energy surface for the change in interplanar angles of butterfly clusters is soft and depends critically on the steric requirements of the ligands spanning the wingtip positions of the butterfly. It is then conceivable that the steric effect imposed by the bulky tricyclohexylphosphine ligands is a possible cause of the conformational change of the M_2Cu_2 metal cores from the planar to the butterfly shape.

Structure of $[PPh_4][Fe_2(CO)_8(\mu\text{-}CuPCy_3)]\cdot 0.5THF$ (4b). The crystal structue of **4b** consists of discrete anions $[Fe_2(CO)_8(\mu\text{-}CuPCy_3)]^-$, cations $[PPh_4]^+$, and disordered THF molecules of solvation. Crystal data are included in Table I. Positional parameters are in Table V, are selected bond distances and angles for the anion are in Table VI. The structure of the anion is shown in Figure 3.

The anion contains a $Fe_2(CO)_8$ unit bridged by a Cu(PCy₃) fragment. The bridging of the Cu(PCy₃) group to the Fe–Fe bond in **4b** distorted the D_{3d} symmetry of the $Fe_2(CO)_8$ unit, as observed in the parent compound $[Fe_2(CO)_8]^{2-}$.[2d,4b] However, the trigonal-bipyramidal coordination geometry for each Fe is still recognizable. The trigonal bipyramid around Fe2 is more distorted than that around Fe1. The Cu atom lies in the plane defined by two Fe atoms and the ligated P atom. There are no bridging carbonyls between two Fe atoms (Fe–C–O bond angles range from 171 to 179°). This structural feature is different from that found in the molecular structures of $[(\mu\text{-}H)Fe_2(CO)_8]^-$[5] and $[Fe_2(CO)_8(\mu\text{-}AuPPh_3)]^-$.[11a] They have two bridging carbonyls as well as a bridging hydride or Au(PPh₃) unit. The Fe–Fe distance in **4b** is 2.900 (2) Å, significantly longer than those in $[(\mu\text{-}H)Fe_2(CO)_8]^-$ (2.521 (1) Å)[5] and $[Fe_2(CO)_8(\mu\text{-}AuPPh_3)]^-$ (2.622 (1) Å),[11]

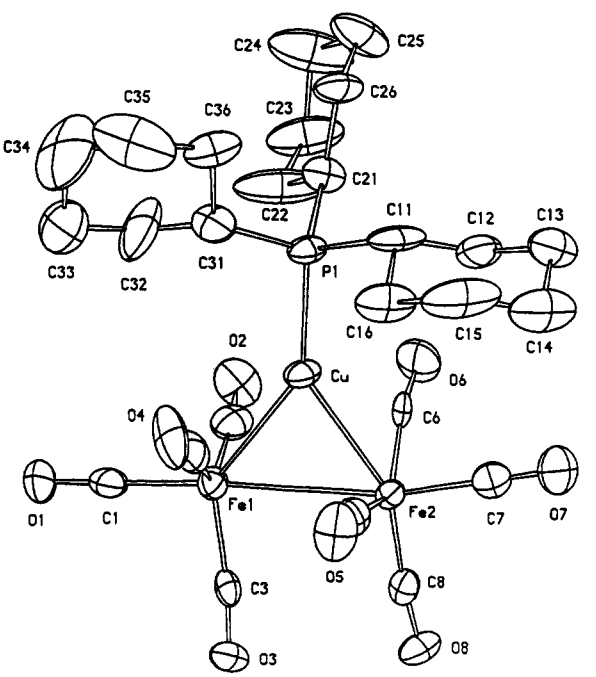

Figure 3. Structure of the anion in $[PPh_4][Fe_2(CO)_8(\mu\text{-}CuPCy_3)]\cdot 0.5THF$ (**4b**·0.5THF) showing the thermal ellipsoids at the 30% probability level. Hydrogen atoms are omitted.

Table VI. Selected Bond Distances (Å) and Bond Angles (deg) for $[PPh_4][Fe_2(CO)_8(\mu\text{-}CuPCy_3)]\cdot 0.5THF$ (4b·0.5THF)

	Distances		
Fe1-Fe2	2.900 (2)	O1-C1	1.15 (1)
Fe1-Cu	2.503 (2)	O2-C2	1.19 (1)
Fe2-Cu	2.487 (2)	O3-C3	1.16 (1)
Cu-P1	2.213 (2)	O4-C4	1.14 (1)
Fe1-C1	1.74 (1)	O5-C5	1.14 (1)
Fe1-C2	1.74 (1)	O6-C6	1.15 (1)
Fe1-C3	1.78 (1)	O7-C7	1.14 (1)
Fe1-C4	1.80 (1)	O8-C8	1.18 (1)
Fe2-C5	1.79 (1)	P1-C11	1.86 (1)
Fe2-C6	1.79 (1)	P1-C21	1.84 (1)
Fe2-C7	1.76 (1)	P1-C31	1.83 (1)
Fe2-C8	1.77 (1)		
	Angles		
Fe2-Fe1-Cu	54.22 (4)	C5-Fe2-C6	140.8 (4)
Fe2-Fe1-C1	174.9 (3)	C5-Fe2-C7	92.7 (4)
Fe2-Fe1-C2	89.6 (3)	C5-Fe2-C8	106.7 (4)
Fe2-Fe1-C3	79.9 (3)	C6-Fe2-C7	90.4 (4)
Fe2-Fe1-C4	93.4 (3)	C6-Fe2-C8	111.3 (4)
Cu-Fe1-C1	130.2 (3)	C7-Fe2-C8	99.3 (4)
Cu-Fe1-C2	78.7 (3)	Fe1-Cu-Fe2	71.05 (5)
Cu-Fe1-C3	132.3 (3)	Fe1-Cu-P1	146.67 (9)
Cu-Fe1-C4	62.6 (3)	Fe2-C7-P1	142.27 (9)
C1-Fe1-C2	89.0 (5)	Cu-P1-C11	111.3 (3)
C1-Fe1-C3	96.4 (4)	Cu-P1-C21	110.6 (3)
C1-Fe1-C4	91.4 (5)	Cu-P1-C31	112.5 (3)
C2-Fe1-C3	117.0 (4)	C11-P1-C21	105.3 (5)
C2-Fe1-C4	128.7 (5)	C11-P1-C31	107.0 (6)
C3-Fe1-C4	114.0 (4)	C21-P1-C31	109.8 (5)
Fe1-Fe2-Cu	54.73 (4)	Fe1-C1-O1	179 (1)
Fe1-Fe2-C5	79.5 (3)	Fe1-C2-O2	174.4 (9)
Fe1-Fe2-C6	87.5 (3)	Fe1-C3-O3	173.6 (8)
Fe1-Fe2-C7	164.6 (3)	Fe1-C4-O4	173 (1)
Fe1-Fe2-C8	95.7 (3)	Fe2-C5-O5	172.8 (9)
Cu-Fe2-C5	77.5 (3)	Fe2-C6-O6	171.2 (8)
Cu-Fe2-C6	65.0 (3)	Fe2-C7-O7	178 (1)
Cu-Fe2-C7	110.8 (3)	Fe2-C8-O8	174.4 (7)
Cu-Fe2-C8	149.5 (3)		

but comparable to the Fe–Fe distances in $[PPh_4]_2[Fe_2(CO)_8]$ (2.792 (1) Å),[4b] $[(Ph_3P)_2N][Fe_2(CO)_8]$ (2.787 (2) Å),[2d] and **1** (2.862 (1) Å). With the bulky PCy_3 ligand, the long Fe–Fe distance may be favored for **4b** in order to ease steric stress and to keep all carbonyl groups in terminal positions.

Structure of $[PPh_4]\{[Fe_2(CO)_8]_2[\mu_4\text{-}\eta^2\text{-}Cu_2(Cy_2PCH_2CH_2PCy_2)]\}$ (7). The unit cell of the crystal structure of **7** contains the hexanuclear dianion $\{[Fe_2(CO)_8]_2[\mu_4\text{-}\eta^2\text{-}Cu_2(Cy_2PCH_2CH_2PCy_2)]\}^{2-}$ and two $[PPh_4]^+$ counterions. The structure of the dianion is shown in Figure 4. The inversion center resides on the midpoint of the ethylene C–C bond in the diphos ligand, and only half of the dianion is in the asymmetric unit. Crystal data are included in Table I. Positional parameters are in Table VII, and selected bond distances and angles for the dianion are in Table VIII.

In the dianion, two $Fe_2(CO)_8$ units are connected by a $CuP(Cy_2)CH_2CH_2(Cy_2)PCu$ fragment. The Fe–Fe distance is 2.8238 (6) Å, which is intermediate between the Fe–Fe distances of **4b** and the parent compound $[Fe_2(CO)_8]^{2-}$.[2d,4b] Fe–Cu distances are normal. The coordination geometry for each Fe atom is similar to that in **4b**. The coordination for Fe1 is, however, more distorted. This distortion may be related to the approach of the C1O1 carbonyl to the Cu atom: The Cu···C1 distance, 2.213 (3) Å, is the shortest Cu–C contact observed in all the structures reported in this paper. The Fe1–C1–O1 angle of 163.8 (3)° is the largest deviation from linearity among **1**, **3**, **4b**, and **7**.

Short Cu···C Contacts in 1, 3, 4b, and 7. Copper–carbon contact distances less than 3 Å are considered to be short;[7] they have been reported for a variety of heterometallic compounds.[7,25] They are also observed in the structures of **1**, **3**, **4b**, and **7**. There are six short Cu···C contacts in **1** and **3**, ranging from 2.388 (6) to 2.650 (5) Å in **1** and from 2.583 (3) to 2.716 (3) Å in **3**. Some Cu···C contacts in **4b** and **7** are even shorter. Four short Cu···C contacts in **4b** are 2.32 (1) Å (Cu···C4), 2.37 (1) Å (Cu···C6), 2.73 (1) Å (Cu···C5), and 2.76 (1) Å (Cu···C2). In addition to 2.213 (3) Å for the Cu···C1 distance, two other short contacts in **7** are Cu···C5 = 2.406 (4) Å and Cu···C6 = 2.391 (3) Å. Crabtree and Lavin[26] classified the bridging carbonyls as symmetrical bridging, bent semibridging, and linear semibridging, the last being further divided into

Table VII. Positional Parameters and Their Estimated Standard Deviations for $[PPh_4]_2\{[Fe_2(CO)_8]_2[\mu_4\text{-}\eta^2\text{-}Cu_2(Cy_2PCH_2CH_2PCy_2)]\}$ (7)[a]

atom	x	y	z	B, Å²
Cu	−0.09220 (4)	0.24865 (4)	−0.12770 (2)	3.519 (9)
Fe1	−0.23818 (5)	−0.30918 (5)	−0.23361 (3)	4.20 (1)
Fe2	0.02847 (5)	0.29868 (5)	−0.24703 (3)	4.54 (1)
P1	−0.04196 (8)	0.19895 (7)	−0.01017 (5)	2.94 (2)
P2	−0.63733 (9)	0.84281 (9)	−0.39018 (5)	3.83 (2)
O1	−0.3035 (3)	0.1376 (3)	−0.1143 (2)	8.47 (9)
O2	−0.2715 (4)	0.5589 (3)	−0.2230 (2)	8.8 (1)
O3	−0.5061 (3)	0.3892 (4)	−0.2711 (2)	10.5 (1)
O4	−0.1578 (5)	0.1841 (4)	−0.3649 (2)	13.4 (1)
O5	0.0608 (4)	0.0434 (3)	−0.2156 (2)	8.1 (1)
O6	−0.0020 (3)	0.4681 (2)	−0.1408 (2)	7.06 (8)
O7	−0.0121 (4)	0.4293 (4)	−0.3956 (2)	10.3 (1)
O8	0.3093 (3)	0.2458 (4)	−0.2725 (3)	13.0 (2)
C1	−0.2635 (4)	0.2055 (4)	−0.1555 (2)	5.5 (1)
C2	−0.2516 (4)	0.4586 (4)	−0.2258 (3)	5.6 (1)
C3	−0.3995 (4)	0.3562 (4)	−0.2552 (3)	6.4 (1)
C4	−0.1844 (5)	0.2336 (5)	−0.3126 (3)	7.6 (1)
C5	0.0418 (4)	0.1459 (4)	−0.2276 (3)	5.7 (1)
C6	0.0053 (4)	0.3994 (3)	−0.1809 (2)	4.9 (1)
C7	−0.0011 (5)	0.3776 (5)	−0.3372 (3)	6.8 (1)
C8	0.1973 (4)	0.2671 (4)	−0.2622 (3)	7.2 (1)
C9	−0.0221 (4)	0.0434 (3)	0.0290 (2)	3.90 (8)
C11	0.1156 (3)	0.2224 (3)	0.0010 (2)	3.35 (8)
C12	0.1490 (4)	0.2116 (3)	0.0813 (2)	4.46 (9)
C13	0.2776 (4)	0.2407 (4)	0.0812 (3)	5.8 (1)
C14	0.3889 (4)	0.1593 (4)	0.0356 (3)	6.4 (1)
C15	0.3563 (4)	0.1673 (3)	−0.0437 (3)	5.1 (1)
C16	0.2286 (3)	0.1398 (3)	−0.0441 (2)	4.17 (9)
C21	−0.1636 (3)	0.2848 (3)	0.0580 (2)	3.51 (8)
C22	−0.1676 (4)	0.4141 (3)	0.0445 (2)	4.8 (1)
C23	−0.2698 (5)	0.4863 (4)	0.0994 (3)	5.8 (1)
C24	−0.4041 (5)	0.4783 (4)	0.0928 (3)	6.7 (1)
C25	−0.4012 (4)	0.3495 (4)	0.1079 (3)	7.5 (1)
C26	−0.2992 (4)	0.2746 (4)	0.0536 (3)	6.2 (1)
C31	−0.7236 (3)	0.9702 (3)	−0.4491 (2)	4.04 (9)
C32	−0.7979 (4)	0.9549 (3)	−0.5012 (2)	4.51 (9)
C33	−0.8719 (4)	1.0540 (4)	−0.5432 (3)	5.8 (1)
C34	−0.8745 (4)	1.1657 (4)	−0.5339 (3)	6.0 (1)
C35	−0.8025 (5)	1.1807 (4)	−0.4821 (3)	6.1 (1)
C36	−0.7248 (4)	1.0835 (4)	−0.4387 (2)	4.9 (1)
C41	−0.5122 (4)	0.7352 (3)	−0.4403 (2)	4.35 (9)
C42	−0.4210 (4)	0.6485 (4)	−0.3996 (2)	5.9 (1)
C43	−0.3295 (5)	0.5591 (5)	−0.4345 (3)	7.1 (1)
C44	−0.3282 (5)	0.5554 (4)	−0.5094 (3)	7.1 (1)
C45	−0.4163 (5)	0.6417 (4)	−0.5498 (3)	6.5 (1)
C46	−0.5107 (4)	0.7325 (4)	−0.5156 (2)	5.0 (1)
C51	−0.5616 (3)	0.8929 (3)	−0.3252 (2)	4.03 (9)
C52	−0.6187 (4)	0.9085 (3)	−0.2542 (2)	4.40 (9)
C53	−0.5637 (4)	0.9575 (4)	−0.2082 (2)	5.6 (1)
C54	−0.4527 (4)	0.9888 (4)	−0.2328 (2)	6.2 (1)
C55	−0.3957 (4)	0.9728 (4)	−0.3030 (3)	6.7 (1)
C56	−0.4486 (4)	0.9248 (4)	−0.3499 (2)	5.8 (1)
C61	−0.7580 (4)	0.7756 (3)	−0.3446 (2)	3.96 (9)
C62	−0.8785 (4)	0.8481 (3)	−0.3190 (2)	4.45 (9)
C63	−0.9746 (4)	0.7993 (4)	−0.2842 (2)	5.6 (1)
C64	−0.9525 (5)	0.6800 (4)	−0.2766 (3)	6.6 (1)
C65	−0.8327 (5)	0.6075 (4)	−0.3011 (3)	6.8 (1)
C66	−0.7342 (4)	0.6529 (4)	−0.3356 (3)	5.5 (1)

[a] See footnote *a* of Table II.

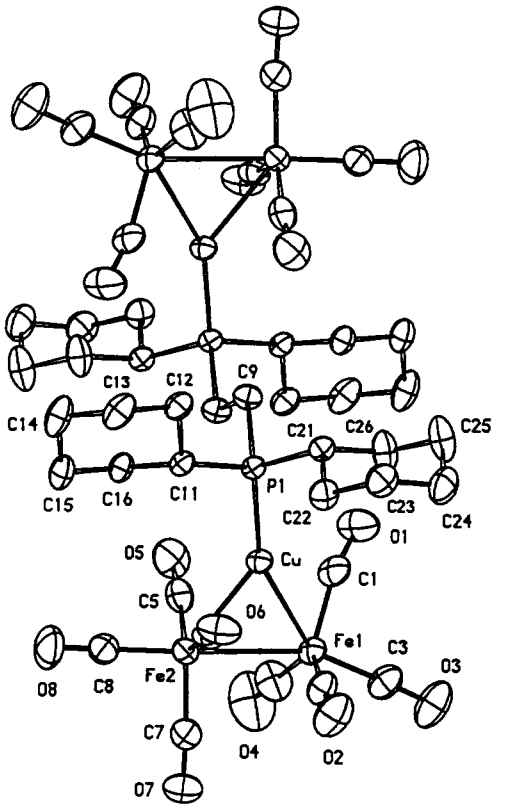

Figure 4. Structure of the dianion in $[PPh_4]_2\{[Fe_2(CO)_8]_2[\mu_4\text{-}\eta^2\text{-}Cu_2(Cy_2PCH_2CH_2PCy_2)]\}$ (7) showing the thermal ellipsoids at the 30% probability level. Hydrogen atoms are omitted.

Scheme I

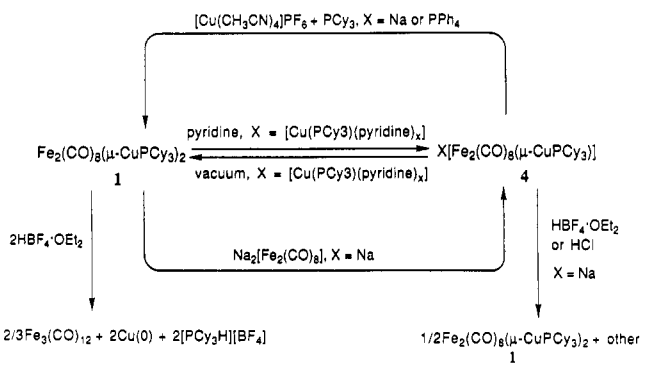

three types (I–III). The C1O1 carbonyl in **7** (Figure 4) is considered to be bent semibridging; the other carbonyls with Cu short contacts in the structures of **1**, **3**, **4b**, and **7** are considered to be type III linear semibridging according to Crabtree and Lavin's criteria.[26] The nature of short Cu···C interactions is still not clear.[7]

The infrared spectra of **4b** and **7** show weak absorptions at 1730–1740 cm^{-1} in both CH_3CN solutions and Nujol mulls (single crystals of **4b** and **7** were used for preparing the samples in Nujol mulls). Since the X-ray structures of **4b** and **7** indicate no bridging carbonyls between the Fe–Fe bonds, we suggest that the very short Cu···C contacts in **4b** and **7** are responsible for these weak absorptions in the solid state. In solution, the possibility that the carbonyls undergo exchange between terminal and bridging positions at the Fe–Fe bonds cannot be discounted, as the infrared spectra of **4b** and **7** are very similar to those of $[Fe_2(CO)_8(\mu\text{-}M'PPh_3)]^-$ (M' = Au, Cu) and the crystal structure of $[Fe_2(CO)_8(\mu\text{-}AuPPh_3)]^-$ indicates two bridging carbonyls.[11a] Nevertheless, only one resonance is observed in the carbonyl region of the ^{13}C NMR spectra for **4b** and **7** even at very low temperature (−60 to −80 °C). The exchange process must be fast on the NMR time scale, as is the case for $[(\mu\text{-}H)Fe_2(CO)_8]^-$.[3e]

Table VIII. Selected Bond Distances (Å) and Angles (deg) for $[PPh_4]_2\{[Fe_2(CO)_8]_2[\mu_4\text{-}\eta^2\text{-}Cu_2(Cy_2PCH_2CH_2PCy_2)]\}$ (7)

Distances			
Fe1–Fe2	2.8238 (6)	O1–C1	1.167 (4)
Fe1–Cu	2.5310 (5)	O2–C2	1.159 (4)
Fe2–Cu	2.4781 (6)	O3–C3	1.153 (4)
Cu–P1	2.2276 (8)	O4–C4	1.157 (5)
Fe1–C1	1.793 (4)	O5–C5	1.168 (5)
Fe1–C2	1.775 (4)	O6–C6	1.161 (4)
Fe1–C3	1.733 (4)	O7–C7	1.148 (5)
Fe1–C4	1.755 (4)	O8–C8	1.151 (5)
Fe2–C5	1.772 (5)	P1–C9	1.844 (3)
Fe2–C6	1.775 (4)	P1–C11	1.854 (3)
Fe2–C7	1.781 (4)	P1–C21	1.851 (1)
Fe2–C8	1.734 (5)	C9–C9	1.524 (4)
Angles			
Fe2–Fe1–Cu	54.80 (2)	C5–Fe2–C6	126.7 (2)
Fe2–Fe1–C1	107.7 (1)	C5–Fe2–C7	121.7 (2)
Fe2–Fe1–C2	79.0 (1)	C5–Fe2–C8	91.6 (2)
Fe2–Fe1–C3	157.5 (2)	C6–Fe2–C7	110.2 (2)
Fe2–Fe1–C4	81.0 (1)	C6–Fe2–C8	96.2 (2)
Cu–Fe1–C1	58.6 (1)	C7–Fe2–C8	94.3 (2)
Cu–Fe1–C2	87.5 (1)	Fe1–Cu–Fe2	68.62 (2)
Cu–Fe1–C3	144.2 (1)	Fe1–Cu–P1	156.89 (3)
Cu–Fe1–C4	117.7 (2)	Fe2–Cu–P1	134.22 (3)
C1–Fe1–C2	123.2 (2)	Cu–P1–C9	116.4 (1)
C1–Fe1–C3	94.8 (2)	Cu–P1–C11	111.3 (1)
C1–Fe1–C4	108.6 (2)	Cu–P1–C21	114.5 (1)
C2–Fe1–C3	88.9 (2)	C9–P1–C11	104.6 (1)
C2–Fe1–C4	127.9 (2)	C9–P1–C21	103.4 (1)
C3–Fe1–C4	92.1 (2)	C11–P1–C21	105.6 (1)
Fe1–Fe2–Cu	56.58 (1)	Fe1–C1–O1	163.8 (3)
Fe1–Fe2–C5	79.2 (1)	Fe1–C2–O2	173.8 (3)
Fe1–Fe2–C6	94.0 (1)	Fe1–C3–O3	178.3 (4)
Fe1–Fe2–C7	85.7 (1)	Fe1–C4–O4	175.3 (4)
Fe1–Fe2–C8	169.1 (2)	Fe2–C5–O5	174.9 (4)
Cu–Fe2–C5	66.6 (1)	Fe2–C6–O6	174.8 (3)
Cu–Fe2–C6	66.0 (1)	Fe2–C7–O7	175.5 (4)
Cu–Fe2–C7	140.5 (1)	Fe2–C8–O8	179.6 (5)
Cu–Fe2–C8	125.1 (2)	P1–C9–C9	113.7 (2)

Scheme II

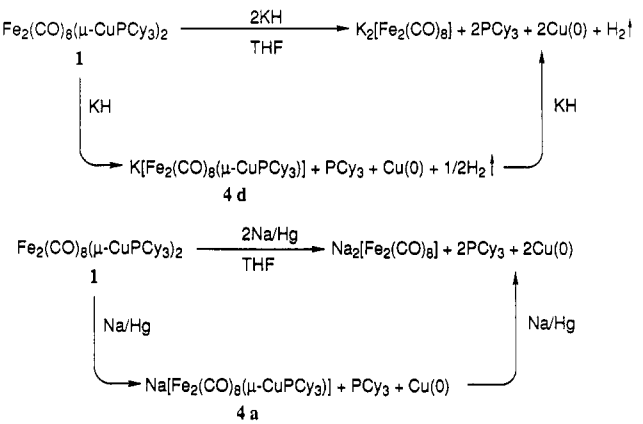

Reactions of 1 and 4. Reactions of **1** and **4** are summarized in Schemes I and II. They are characterized by the transformations between species **1** and **4** and the ready reduction of Cu(I) in the clusters to Cu(0).

The PR_3-promoted dissociation of the $M'(PR_3)$ unit from a mixed-metal cluster has been observed for some clusters.[7] When **1** is treated with 3 equiv of PCy_3, dissociation does not occur. When **1** is dissolved in pyridine, however, the green color of the solid turns to red in solution. Its infrared spectrum in pyridine is almost identical with that of **4b** in CH_3CN. The ^{13}P and ^{13}C NMR spectroscopic data also suggest that **1** reacts with pyridine to produce [Cu-

$(PCy_3)(pyridine)_x][Fe_2(CO)_8(\mu\text{-}CuPCy_3)]$ (**4c**). Pyridine can be removed by prolonged pumping under high vacuum, and **1** is recovered.

Addition of 1 equiv of $[Cu(CH_3CN)_4]PF_6$ and PCy_3 to **4b** also yields **1**. On the other hand, the reaction between **1** and $Na_2[Fe_2(CO)_8]$ in THF results in **4a**. Sodium amalgam reacts with **1** to reduce Cu(I) in the cluster to Cu(0). The overall reaction proceeds in two steps as shown in Scheme II. Similarly, the reaction of **1** with KH reduces Cu(I) and proceeds in two steps. In both reactions above, the intermediate products are sodium and potassium salts of **4** (**4a,d**).

Both **1** and **4** are protonated by $HBF_4{\cdot}OEt_2$. Protonation of **1** causes the reduction of Cu(I) to Cu(0) and the oxidation of $[Fe_2(CO)_8]^{2-}$ to $Fe_3(CO)_{12}$. Protonation of **4a** with 1 equiv of $HBF_4{\cdot}OEt_2$ produces $^1/_2$ equiv of **1** and a mixture of intractable materials. Protonation of **4a** with HCl was also performed in THF-d_8 at −80 °C. The reaction was monitored by variable-temperature ^1H and ^{31}P NMR spectroscopy. The attempt to observe possible intermediate products $[(\mu\text{-}H)Fe_2(CO)_8(\mu\text{-}CuPCy_3)]$ and $H_2Fe_2(CO)_8$ failed; instead, **1** was observed even at −80 °C. The other products or decomposed material could not be definitely identified.

Acknowledgment. This work was supported by the National Science Foundation through Grant CHE88-00515. NMR spectra were obtained at the Ohio State University Campus Chemical Instrument Center funded in part by NSF Grant 79-10019 and NIH Grant 1 S10 PR0140518-01A. H.D. thanks BP America for a fellowship.

Supplementary Material Available: Listings of calculated hydrogen atom positional parameters, anisotropic thermal parameters, bond distances, and bond angles for **1**, **3**, **4b**·0.5THF, and **7** (28 pages); listings of structure factor amplitudes (168 pages). Ordering information is given on any current masthead page.

Palladium(II)-Catalyzed Exchange and Isomerization Reactions. 14.[1] Kinetics and Stereochemistry of the Isomerization and Water Exchange of 2-(Methyl-d_3)-4-methyl-1,1,1,5,5,5-hexafluoro-3-penten-2-ol in Aqueous Solution Catalyzed by $PdCl_4^{2-}$: Two New Mechanistic Probes for Catalytic Chemistry

John W. Francis and Patrick M. Henry*

Department of Chemistry, Loyola University of Chicago, Chicago, Illinois 60626

Received February 7, 1991

The isomerization of 2-(methyl-d_3)-4-methyl-1,1,1,5,5,5-hexafluoro-3-penten-2-ol (**2a**) into an equilibrium mixture of **2a** and 2-methyl-4-(methyl-d_3)-1,1,1,5,5,5-hexafluoro-3-penten-2-ol (**2b**) in aqueous solution was studied by ^1H and ^2H NMR, under the Wacker conditions of low chloride (<1.0 M) and acid (<0.5 M) concentrations. The rate expression under these conditions is rate = $k_i[PdCl_4^{2-}][\mathbf{2a}]/[H^+][Cl^-]^2$, with $k_i = 1.05 \times 10^{-6}$ s^{-1}. The exchange of **2a** with ^{18}O-enriched water was studied by ^{13}C NMR using isotope-induced shift methods and the rate of exchange was found to be the same as the rate of isomerization within experimental error. This result requires that isomerization and exchange occur by a hydroxypalladation route, rather than through palladium(IV)-π-allyl intermediates. The rate expression for isomerization at low chloride concentrations is identical with the rate expression for the Wacker oxidation of ethene to acetaldehyde. This result is inconsistent with a proton inhibition arising from equilibrium hydroxypalladation but is consistent with proton loss from the Pd(II) coordination sphere in a preequilibrium step followed by a cis hydroxypalladation occurring from within the coordination sphere of the palladium(II). Stereochemical studies were conducted with chiral (*E*)-**2a**. The observed result was the formation of chiral **2b** with the opposite configuration of the initial **2a**. This result is also consistent only with cis hydroxypalladation; so both kinetic and stereochemical mechanistic probes give the same result.

Introduction

The fact that most catalytic reactions involve several steps makes the interpretation of kinetic data in terms of mechanisms ambiguous in such complicated systems. For instance, in the Wacker process for the oxidation of olefins to aldehydes and ketones in aqueous solution by $PdCl_4^{2-}$, the kinetic rate expression, given by eq 1, can be interpreted in several ways. Although most workers agree the $[Cl^-]^2$ inhibition results from displacement of two chlorides by olefin and water in the Pd(II) coordination sphere in rapid preequilibria, there is considerable disagreement as to the source of the proton inhibition. The kinetics are consistent with (a) cis addition by coordinated hydroxyl in the slow step, eq 2, or (b) trans attack by external water in an equilibrium step, eq 3.[2] In the second mechanism, decomposition of the adduct is rate determining.

$$\text{rate} = k[PdCl_4^{2-}][\text{olefin}]/[H^+][Cl^-]^2 \qquad (1)$$

The arguments in favor of one or the other of the proposed mechanisms are based on (1) stereochemical results,[3-5] (2) comparisons of kinetic and competitive isotope

(1) Part 13: Dumlao, C. M.; Francis, J. W.; Henry, P. M. *Organometallics* **1991**, *10*, 1400.

(2) For a general discussion and references: Henry, P. M. *Palladium Catalyzed Oxidation of Hydrocarbons*; D. Reidel: Dordrecht, Holland, 1980; pp 41-84.

(3) Stille, J. K.; James, D. E. *J. Organomet. Chem.* **1976**, *108*, 401.

0276-7333/91/2310-3498$02.50/0